ACS Catalysis

Research Article

pubs.acs.org/acscatalysis

Agglomerative Sintering of an Atomically Dispersed Ir_1/Zeolite Y Catalyst: Compelling Evidence Against Ostwald Ripening but for Bimolecular and Autocatalytic Agglomeration Catalyst Sintering Steps

Ercan Bayram,[†,⊥] Jing Lu,[‡] Ceren Aydin,[‡] Nigel D. Browning,[‡,§] Saim Özkar,[∥] Eric Finney,[†] Bruce C. Gates,[*,‡] and Richard G. Finke[*,†]

[†]Department of Chemistry, Colorado State University, Fort Collins, Colorado 80523, United States

[‡]Department of Chemical Engineering and Materials Science, University of California, Davis, One Shields Avenue, Davis, California 95616, United States

[§]Fundamental and Computational Sciences, Pacific Northwest National Laboratory, 902 Battelle Blvd, Richland, Washington 99352, United States

[∥]Department of Chemistry, Middle East Technical University, 06800 Ankara, Turkey

Supporting Information

ABSTRACT: Agglomerative sintering of an atomically dispersed, zeolite Y-supported catalyst, Ir_1/zeolite Y, formed initially from the well-characterized precatalyst $[Ir(C_2H_4)_2]$/zeolite Y and in the presence of liquid-phase reactants, was monitored over three cycles of 3800 turnovers (TTOs) of cyclohexene hydrogenation at 72 °C. The catalyst evolved and sintered during each cycle, even at the relatively mild temperature of 72 °C in the presence of the cyclohexene plus H_2 reactants and cyclohexane solvent. Post each of the three cycles of catalysis, the resultant sintered catalyst was characterized by extended X-ray absorption fine structure spectroscopy and atomic-resolution high-angle annular dark-field scanning transmission electron microscopy. The results show that higher-nuclearity iridium species, Ir_n, are formed during each successive cycle. The progression from the starting mononuclear precursor, Ir_1, is first to $Ir_{\sim 4-6}$; then, on average, $Ir_{\sim 40}$; and finally, on average, $Ir_{\sim 70}$, the latter more accurately described as a bimodal dispersion of on-average $Ir_{\sim 40-50}$ and on-average $Ir_{\sim 1600}$ nanoparticles. The size distribution and other data disprove Ostwald ripening during the initial and final stages of the observed catalyst sintering. Instead, the diameter-dispersion data plus quantitative fits to the cluster or nanoparticle diameter vs time data provide compelling evidence for the underlying, pseudoelementary steps of bimolecular agglomeration, B + B → C, and autocatalytic agglomeration, B + C → 1.5C, where B represents the smaller, formally Ir(0) nanoparticles, and C is the larger (more highly agglomerated) nanoparticles (and where the 1.5 coefficient in the autocatalytic agglomeration of B + C necessarily follows from the definition, in the bimolecular agglomeration step, that 1C contains the Ir from 2B). These two specific, balanced chemical reactions are of considerable significance in going beyond the present state-of-the-art, but word-only, "mechanism"—that is, actually and instead, just a collection of phenomena—for catalyst sintering of "Particle Migration and Coalescence". The steps of bimolecular plus autocatalytic agglomeration provide two specific, balanced chemical equations useful for fitting sintering kinetics data, as is done herein, thereby quantitatively testing proposed sintering mechanisms. These two pseudoelementary reactions also define the specific words and concepts for sintering of bimolecular agglomeration and autocatalytic agglomeration. The results are also significant as the first quantitative investigation of the agglomeration and sintering of an initially atomically dispersed metal on a structurally well-defined (zeolite) support and in the presence of liquid reactants (cyclohexene substrate and cyclohexane solvent) plus H_2. A list of additional specific conclusions is provided in a summary section.

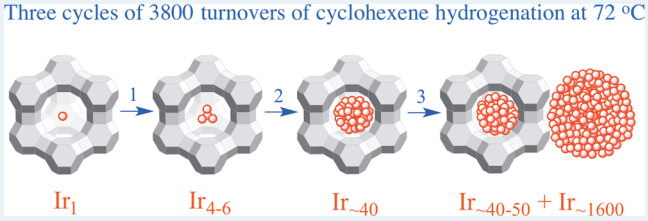

KEYWORDS: *catalyst, sintering, agglomeration, kinetics, Ostwald ripening, nanoparticle, cluster, mononuclear*

INTRODUCTION

Sintering of a supported catalyst[1−12] is that sum of processes whereby (i) catalyst agglomeration occurs with an accompanying loss of catalytic surface area and, hence, loss of activity; whereby (ii) collapse of the catalyst support occurs;[13] or whereby (iii) both of these (and any other) processes occur that limit a catalyst's lifetime, reduce a catalyst's productivity, increase the net final cost of the catalyst, and result in increased energy use.[3,5] Ostwald ripening (OR) is often believed to be an underlying process involved in catalyst sintering and involves the breakup of a typically smaller metal particle into a single-atom fragment, $M_n \rightarrow M_1 + M_{n-1}$, followed by M_1 migration and agglomeration with a second, larger, particle, M_m, namely, $M_1 + M_m \rightarrow M_{m+1}$, in a net process $M_n + M_m \rightarrow M_{n-1} + M_{m+1}$ that is initially

Received: February 14, 2015
Revised: April 15, 2015
Published: May 12, 2015

DOI: 10.1021/acscatal.5b00321
ACS Catal. 2015, 5, 3514−3527

size-defocusing/broadening and ultimately yields larger, lower-surface-area particles that are typically less active catalytically.[14−19] The other most often cited (but in words only) "mechanism" of particle sintering is particle migration and coalescence (PMC),[1,3−5,7] although the precise balanced chemical equations that constitute PMC are typically not given and, therefore, unclear. Restated, PMC cannot possibly be a true mechanism because it does not contain any specific, balanced chemical equations that can be used to, for example, curve-fit kinetics data. Instead, PMC is simply a collection of observations and phenomena. Moreover, and unfortunately, such putative mechanistic processes are often assumed and not independently checked by experiment.[20,21]

Atomically dispersed precatalysts[13,14,22−28] such as the well-characterized mononuclear iridium complexes supported on zeolite HY employed herein, shown in Figure 1 and abbreviated as $[Ir_1]$/zeolite Y,[14,15,17,29,30] offer a unique, previously unexploited opportunity to test the stability of atomically dispersed catalysts. They also offer an unprecedented opportunity to observe metal agglomeration and sintering from an initially atomically dispersed catalyst that cannot, at least initially, undergo OR[17−19,30] because the initial fragmentation process $M_n \rightarrow M_1 + M_{n-1}$ is not possible for $n = 1$ (i.e., atomically dispersed M_1 catalysts such as our $[Ir_1]$/zeolite Y). Indeed, investigation of the early stages of agglomeration of our atomically dispersed catalyst also offers a unique opportunity to probe several open questions, including (a) What is the stability toward sintering of such atomically dispersed catalysts? (b) What is the time profile (kinetics) of the reaction at each stage of sintering beginning from a mononuclear species as it catalyzes a prototype, simple reaction such as cyclohexene hydrogenation? Are there, for example, (re)activation/induction periods, or is the catalyst immediately active? (c) How does the initial rate at each stage correlate with the number of accessible metal atoms of the agglomerating catalyst? (d) What are the observable stages of agglomeration, n, in terms of the metal product, Ir_n, post a few thousand cycles of catalysis? And (e) what is the role of the liquid phase, solvent and other reactants (in what follows, cyclohexene and H_2)?

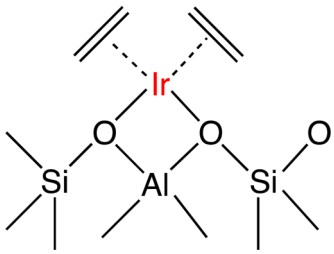

Figure 1. Schematic representation of the structure of the $[Ir(C_2H_4)_2]$/zeolite Y precatalyst prepared by the reaction of $[Ir(C_2H_4)_2(acac)]$ (acac: $CH_3COCH_2COCH_3$) with highly dealuminated (Si/Al = 30) zeolite Y. Each Ir atom is π-bonded to two ethylene ligands and anchored to the support by two Ir−O bonds, as in the precursor $[Ir(C_2H_4)_2(acac)]$. Reprinted with permission from ref 31. Copyright 2012, American Chemical Society.

Recent Investigations of the $[Ir(C_2H_4)_2]$/Zeolite Y Precatalyst in Contact with Solution: Demonstration of An Initially Atomically Supported Ir_1 as the True Catalyst. In a recent collaboration between our Colorado State University (CSU) and UC Davis (UCD) groups,[31] we examined the site-isolated, mononuclear zeolite-supported precatalyst $[Ir(C_2H_4)_2]$/zeolite Y (Figure 1).[14,15,17,29,30] Our recent collaborative focus[31] was on the question of "what is the true catalyst for cyclohexene hydrogenation *at 22 °C*; specifically, is it the initial mononuclear, atomically dispersed $[Ir_1]$/zeolite Y species?" Evidence providing strong support for retention of the atomic dispersion of the iridium at 22 °C included[31] (i) the kinetics of our reporter reaction (especially the lack of an observable induction period during which higher-nuclearity aggregates could have formed),[31] postcatalysis extended X-ray absorption fine structure (EXAFS) spectra of the resultant iridium species (indicating no detectable Ir−Ir contributions, consistent with mononuclear iridium),[31] and high-angle annular dark-field scanning transmission electron microscopy (HAADF-STEM) images indicating only atomically dispersed iridium on the support.[31] Moreover, (ii) quantitative catalyst poisoning experiments with $P(OCH_3)_3$ showed that 1.0 equiv of $P(OCH_3)_3$ per equivalent of Ir completely halted the catalytic activity, providing compelling evidence for an intrazeolite, mononuclear $[Ir_1]$/zeolite Y catalyst with no detectable metal leaching into solution.[31] The conclusion of the $[Ir_1]$ catalyst within the zeolite Y pore structure was bolstered by (iii) the lack of detectable poisoning by the larger $P(C_6H_{11})_3$, a ligand too large to enter the pores.[31] In short, the results constitute a rare example wherein all the evidence necessary to identify unequivocally an atomically dispersed, supported transition-metal species as the true catalyst was obtained.[31] The significance of that work for the present studies is that it pins down atomically dispersed $[Ir_1]$/zeolite Y as the starting point of the catalyst sintering investigation detailed herein.

Preliminary Studies at Higher Temperatures. In our prior work,[31] we also performed initial cyclohexene hydrogenation survey experiments starting with the site-isolated, mononuclear zeolite-supported precatalyst $[Ir(C_2H_4)_2]$/zeolite Y at 50 °C. The goal of those survey experiments was to determine whether the atomic dispersion was retained at temperatures above 22 °C. The data suggested, instead, that the initially formed, mononuclear $[Ir_1]$/zeolite Y catalyst slowly evolved to higher-nuclearity species, even at the mild temperature of 50 °C and in the presence of the liquid reactant, cyclohexene, H_2, and cyclohexane solvent. Hence, that preliminary observation opened up the possibility of quantitatively investigating the sintering of the initially atomically dispersed, prototype $[Ir_1]$/zeolite Y catalyst system[31] under liquid-phase conditions.

Herein, we report the results of experiments at 72 °C whereby catalyst agglomerative sintering is faster than at 50 °C but still observable in discrete stages. We characterized the sintering of the initially $[Ir_1]$/zeolite Y catalyst following each of three cycles of 3800 total turnovers (TTOs, = 4.94 mmol cyclohexene/1.3 μmol Ir) of cyclohexene hydrogenation in the liquid phase. We have monitored the initial rate of reaction at each stage and characterized the several postcatalysis samples by HAADF-STEM and EXAFS spectroscopy.[18] In a nutshell, the data demonstrate the agglomerative sintering of the initial Ir_1 species at 72 °C to sequentially yield (i) clusters well approximated as $Ir_{\sim 4-6}$ following the first 3800 TTOs occurring over 2 days, then (ii) on-average $Ir_{\sim 40}$ clusters after 7600 TTOs, and then (c) on-average $Ir_{\sim 70}$ clusters, that are more accurately described as a bimodal distribution of on-average $Ir_{\sim 40-50}$ and on-average $Ir_{\sim 1600}$ nanoparticles, after 11 400 TTOs of cyclohexene. The total of 11 400 TTOs of catalysis were accompanied by an overall 8.1-fold decrease in the initial rate of hydrogenation. The results and the analysis that follows are of considerable interest because they provide (i) the first quantitative characterization of the

DOI: 10.1021/acscatal.5b00321
ACS Catal. 2015, 5, 3514−3527

agglomerative sintering of an atomically dispersed catalyst; (ii) compelling evidence against Ostwald ripening; and (iii) an identification and employment of the specific, balanced chemical reaction, pseudoelementary mechanistic steps of bimolecular agglomeration, B + B → C, and autocatalytic agglomeration, B + C → 1.5C, to account for the agglomeration average particle size vs time data quantitatively.

RESULTS AND INITIAL DISCUSSION

First Cycle of 3800 Turnovers of Cyclohexene Hydrogenation Starting with $[Ir(C_2H_4)_2]$/Zeolite Y at 72 °C: Kinetics and Post-Kinetics EXAFS and HAADF-STEM Analyses. *Reaction Kinetics and Initial Rates.* Figure 2 shows the kinetics data starting initially with the $[Ir(C_2H_4)_2]$/zeolite-Y precatalyst under what we refer to as standard conditions, that is, 72.0 ± 0.1 °C, 3800 equiv of cyclohexene (relative to 1 equiv of Ir) in cyclohexane solvent, all in a batch reactor prepared in an N_2-filled drybox. The reactor with the precatalyst was removed from the drybox and attached to a hydrogenation line equipped with a computer-interfaced pressure transducer for monitoring the decreasing H_2 partial pressure as a measure of the conversion of the cyclohexene, which is known to react with H_2 in a 1:1 stoichiometry to yield cyclohexane.[32] The catalysis experiment was started by pressuring the system with H_2 to 40 ± 1 psig and vortex-stirring to keep the catalyst particles suspended.

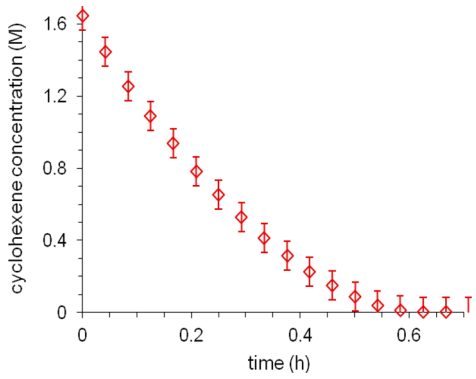

Figure 2. First cycle of 3800 TTOs of cyclohexene hydrogenation under standard conditions (◊) at 72.0 ± 0.1 °C. The cyclohexene concentrations were calculated from H_2 uptake data determined by measuring the H_2 partial pressure loss then converting to the loss of cyclohexene by the known 1:1 H_2-to-cyclohexene stoichiometry.[32] For clarity, only one of every five datum points is shown.

The kinetics data over the first cycle of 3800 TTOs of cyclohexene hydrogenation are shown in Figure 2, plotted as cyclohexene concentration vs time. A cyclohexene plus cyclohexane (reactant plus solvent) vapor-pressure correction was applied to determine accurate changes in the H_2 partial pressure during the reaction, as described elsewhere[33] (see the Supporting Information for details of the vapor pressure correction).

Noteworthy is that the cyclohexene hydrogenation reaction started immediately, without a detectable induction period, which is consistent with the starting $[Ir(C_2H_4)_2]$/zeolite-Y precatalyst rapidly evolving to a kinetically competent catalyst. The hydrogenation took only about 40 min to completely consume 100% of the limiting reactant, cyclohexene. The cyclohexene hydrogenation curve in Figure 2 is very similar to the one obtained for the same reaction at 22.0 ± 0.1 °C,[31] with the only notable difference being the ∼12-fold increased rate of hydrogenation, the complete hydrogenation (3800 turnovers) requiring only 40 min at 72 °C (vs 480 min at 22 °C).[31]

The initial rate of cyclohexene hydrogenation in the first cycle, determined from the slope of the curve at time zero (Figure 2), is 4.4 M/h for the standard catalyst mass that was employed (in what follows, we use this same basis for representing reaction rates). Repeat experiments showed that this value was reproducible within an error of ±5%.

Lack of a Detectable Induction Period and the Important Associated Definition of the Sintering Starting Point. An important observation in this first cycle of hydrogenation catalysis is the lack of any detectable induction period or associated sigmoidal kinetics curve. If present, then such sigmoidal kinetics would most likely have been characteristic of the two-step mechanism of nanoparticle nucleation and autocatalytic growth, A → B, A + B → 2B (where, in the present example, A = Ir^I/zeolite Y and B = Ir(0) or, perhaps, Ir−H, plus probably other ligands as well).[32] What this means, in turn, is that later in the paper, when we fit the agglomerated nanoparticle diameter vs time data, we should (and will) use the nomenclature indicating that we are starting with "B", that is, formally Ir(0), in the agglomerative sintering process, not "A", the Ir^I/zeolite Y precatalyst.

Characterization of the Resultant Catalyst. Ex situ EXAFS and HAADF-STEM characterizations of the catalyst were carried out, after the first cycle of 3800 TTOs,[18] with the primary goal of establishing the nuclearity, *n*, of the resultant Ir_n catalyst. The EXAFS best-fit model characterizing the postcatalysis sample is given in Table 1 (see the Supporting Information for data characterizing the other two models tested in detail in the EXAFS data fitting). Significantly, the EXAFS spectra indicate that only mononuclear iridium species, Ir_1, are present, with the best-fit Ir−Ir coordination number being indistinguishable from zero. The Ir−C and Ir−C_{long} coordination numbers[34] are 5.7 and 3.7, and the Ir−$O_{zeolite}$ and Ir−Al coordination numbers are 2.0 and 1.0, respectively, showing again that, on average and within experimental error, each Ir atom in the catalyst after 3800 TTOs is still bonded to two oxygen atoms at the aluminum site of the zeolite and has ligands with low-atomic-number atoms, which we infer to be carbon.

Table 1. Summary of EXAFS Data at the Ir L_{III} Edge Characterizing the Catalyst Formed from the Starting $[Ir(C_2H_4)_2]$/Zeolite Y and Following the First 3800 TTOs of Cyclohexene Hydrogenation at 72.0 ± 0.1 °C

	EXAFS parameters[a]			
absorber−backscatterer pair	*N*	*R* (Å)	$10^3 \times \Delta\sigma^2$ (Å^2)	ΔE_0 (eV)
Ir−$O_{zeolite}$	2.0	2.23	2.0	−7.8
Ir−C	5.7	2.15	6.8	−7.6
Ir−Al	1.0	3.08	0.7	−2.4
Ir−C_{long}	3.7	3.06	1.0	−8.0
Ir−Ir	*b*	*b*	*b*	*b*

[a]Notation: *N*, coordination number; *R*, distance between absorber and backscatterer atoms; $\Delta\sigma^2$, variance in the absorber−backscatterer distance (Debye−Waller factor); ΔE_0, inner potential correction. Error bounds (accuracies) characterizing the parameters are estimated to be as follows: *N*, ± 20%; *R*, ± 0.02 Å; $\Delta\sigma^2$, ± 20%; and ΔE_0, ± 20%. [b]Contribution not detectable. Details of the EXAFS data fitting are provided in the Supporting Information.

DOI: 10.1021/acscatal.5b00321
ACS Catal. 2015, 5, 3514−3527

Because the errors in the EXAFS data (e.g., ± 20% in coordination numbers) imply that low concentrations of higher-nuclearity iridium species Ir_n, $n > 1$, could have been missed by the EXAFS analysis in samples that contained predominantly Ir_1 complexes, HAADF-STEM imaging was performed with the same postkinetics sample used in the EXAFS experiments. The results (Figure 3) confirm the principal findings of the EXAFS analysis by showing that the sample is still composed of primarily isolated mononuclear Ir_1 species. However, significantly, two small subnanometer iridium clusters with diameters of ∼0.42 and 0.45 nm, approximated as Ir_4, are identified in the image, Ir_4 clusters being known to be stable in this system and to form from the mononuclear species.[19]

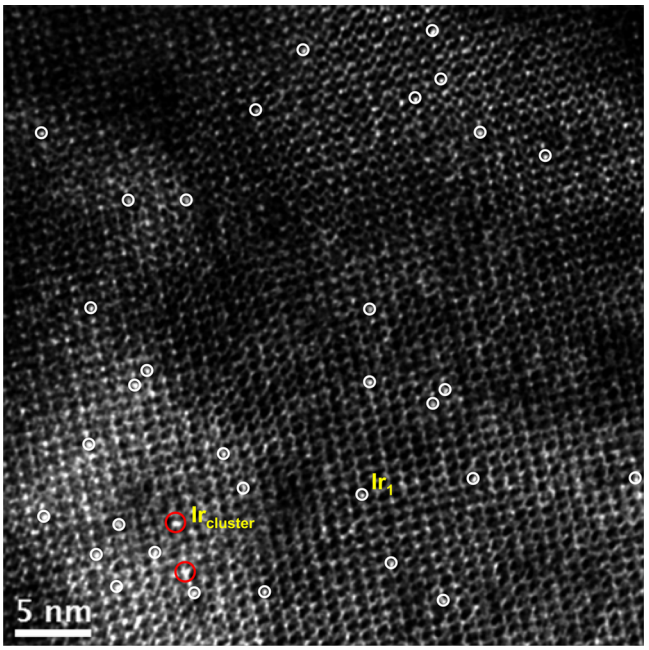

Figure 3. HAADF-STEM image of the postcatalysis sample formed from the $[Ir(C_2H_4)_2]$/zeolite Y precatalyst and following the first 3800 TTOs of cyclohexene hydrogenation at 72.0 ± 0.1 °C. In the HAADF imaging mode, the iridium species appear as bright features as a consequence of the *Z* (atomic number)-contrast between the heavy Ir atoms and the zeolite Y framework, which incorporates only light elements. The image shows that the iridium is still present primarily as isolated mononuclear, Ir_1, complexes, as indicated by the isolated Ir atoms (some examples are circled in white). Notable, however, is that two iridium clusters with subnanometer diameters of ∼0.42 and 0.45 nm are also evident (circled in red), corresponding to $Ir_{\sim 4}$ clusters.[19] Hence, this image provides evidence of an early stage of $Ir_{\sim 4}$ cluster formation.

Formation of an $Ir_{\sim 4-6}$/zeolite Y Catalyst Plus Its EXAFS and HAADF-STEM Characterization. Another standard conditions, 3800 TTOs cyclohexene hydrogenation experiment at 72.0 ± 0.1 °C was carried out beginning with fresh $[Ir(C_2H_4)_2]$/zeolite Y, but after those 3800 TTOs, the reactor was kept on the H_2 line for ∼2 days at 72.0 ± 0.1 °C[35] under the ∼25 psig that remained[36] (after the conversion of 3800 equiv of cyclohexene) to allow the what turned out to be $Ir_{\sim 4-6}$ clusters (vide infra) to fully evolve. The EXAFS data representing the best-fit model characterizing the sample after this experiment (details in Supporting Information) are shown in Table 2. Significantly, the data indicate an average Ir−Ir coordination number of 2.9, consistent with the predominance of tetrahedral Ir_4 clusters, which are known to be relatively stable.[17,20,21,37−39] The average Ir−Ir bond distance of 2.67 Å is typical for Ir_4.[17,20,21,37−39] The Ir−C and Ir−C_{long} coordination numbers[34] (4.1 and 4.0, respectively) are consistent with the presence of hydrocarbon ligands. The Ir−$O_{support}$ coordination number decreased from ∼2 for the mononuclear species to 0.5, indicating the unlinking of iridium from the support, as expected for such cluster formation.[17]

Table 2. Summary of EXAFS Data at the Ir L_{III} Edge, Characterizing the Sample Formed from $[Ir(C_2H_4)_2]$/Zeolite Y after Cyclohexene Hydrogenation at 72.0 ± 0.1 °C after 3800 TTOs of Cyclohexene Hydrogenation, Followed by ∼2 Days under H_2, As Described in the Text

	EXAFS parameters[a]			
absorber−backscatterer pair	*N*	*R* (Å)	$10^3 \times \Delta\sigma^2$ (Å^2)	ΔE_0 (eV)
Ir−$O_{zeolite}$	0.51	2.10	1.5	−2.9
Ir−C	4.1	2.27	11	−7.5
Ir−C_{long}	4.0	3.09	0.73	5.3
Ir−Ir	2.9	2.67	6.3	−5.5

[a]Notation: *N*, coordination number; *R*, distance between absorber and backscattering atoms; $\Delta\sigma^2$, variance in the absorber−backscatterer distance; ΔE_0, inner potential correction. Error bounds (accuracies) characterizing the parameters are estimated to be as follows: *N*, ± 20%; *R*, ± 0.02 Å; $\Delta\sigma^2$, ± 20%; and ΔE_0, ± 20%. Details of the EXAFS data fitting are provided in the Supporting Information.

HAADF-STEM images of this sample provide further evidence of iridium clusters, with a mean diameter of 0.45 ± 0.12 nm for 145 counted particles (Figure 4). The histogram given in Figure 4 shows that the evolved iridium clusters are characterized by a narrow, unimodal, and empirically nearly Gaussian size distribution. The 0.45 nm mean diameter is within the ranges reported on the basis of HAADF-STEM images of Ir_4 and Ir_6 clusters, namely, 0.39 ± 0.03 and 0.49 ± 0.03 nm, respectively, with narrow size dispersities of ±7.6% and 6.1%, respectively.[40] A slight overestimation of the cluster diameters is expected on the basis of precedented blurring effects in HAADF-STEM imaging associated with the electron beam probe size, vibrational instabilities, irradiation effects, off-focus, and beam broadening,[41] but the histogram of *relative sizes* is expected to be accurate. The absence of a second-shell Ir−Ir contribution in the EXAFS data is evidence against the presence of a substantial fraction of octahedral Ir_6 clusters in the sample, but the images do indicate the presence of a few Ir_6 clusters (which are also known to be quite stable[42]). Overall, the product can be labeled with some confidence as $Ir_{\sim 4-6}$/zeolite Y. Although it is difficult to know if we have complete mass balance in our product studies, the combination of a bulk (EXAFS) with a microscopic (HAADF-STEM) method implies that we are seeing most if not all of the main products formed during the catalysis and associated sintering.

The bottom line is that the EXAFS and HAADF-STEM evidence demonstrates that the additional ∼2 days of treatment under H_2, in contact with cyclohexane solution at 72.0 ± 0.1 °C, resulted in the transformation of the primarily Ir_1/zeolite Y catalyst into one that is well approximated as $Ir_{\sim 4-6}$/zeolite Y.

Second Cycle of 3800 TTOs of Cyclohexene Hydrogenation Beginning with the $Ir_{\sim 4-6}$/Zeolite Y Catalyst: Kinetics and HAADF-STEM Evidence of Sintering To Form $Ir_{\sim 40}$ Nanoparticles. The evolved, now $Ir_{\sim 4-6}$/zeolite Y, catalyst was subjected to a second cycle of 3800 TTOs of cyclohexene hydrogenation at 72.0 ± 0.1 °C and 40 ± 1 psig initial H_2 partial

DOI: 10.1021/acscatal.5b00321
ACS Catal. 2015, 5, 3514−3527

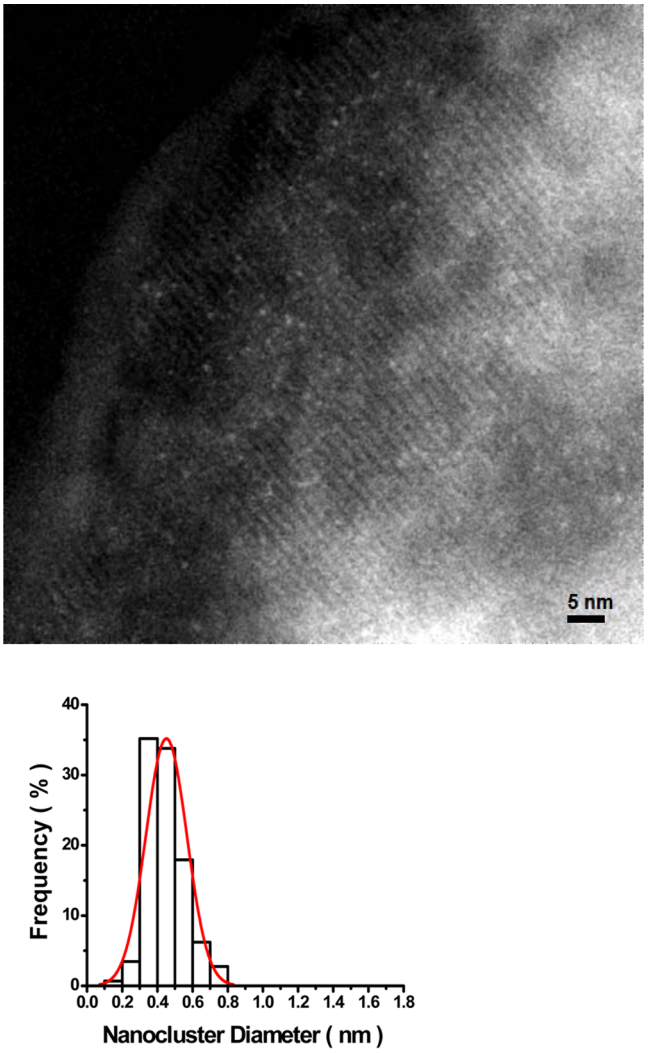

Figure 4. (top) HAADF-STEM image of the catalyst after cyclohexene hydrogenation that was kept under the remaining, ~25 psig H_2 partial pressure for an additional ~2 days at 72.0 ± 0.1 °C. (bottom) Distribution of diameters measured for 145 iridium clusters. The mean cluster diameter of 0.45 ± 0.12 nm corresponds primarily to Ir_4 clusters, but with a few Ir_6 clusters present, as discussed in the main text. The red line represents an empirical Gaussian curve-fit (OriginPro software) to the distribution of the cluster diameters.

pressure as detailed in the Experimental Methods and Data Analysis section. As shown in Figure 5, the catalysis began immediately, again without any detectable induction period, as expected because a preformed $Ir_{\sim 4-6}$/zeolite Y catalyst is present. The initial rate of cyclohexene hydrogenation in this second cycle was found to be 1.3 M/h, with an error of ±10% determined in repeat experiments.

HAADF-STEM images of this post-7600 TTOs catalyst demonstrate the presence of now even larger and more broadly dispersed nanoparticles, with an average diameter of 1.04 ± 0.22 nm (±21%) for the 98 counted particles, corresponding on-average to $Ir_{\sim 40}$ (Figure 6).[43] These results are in good agreement with earlier observations of the enhanced stability of iridium clusters of this size,[44] $Ir_{\sim 40}$, which are resistant to further sintering.[45] Strikingly, recent studies by one of our groups, of so-called Ziegler-type nanoparticles stabilized by $AlEt_3$, also show a constant size of precisely (on average) $Ir_{\sim 40}$ for that system and its rather different stabilizer.[46] These and additional results[45]

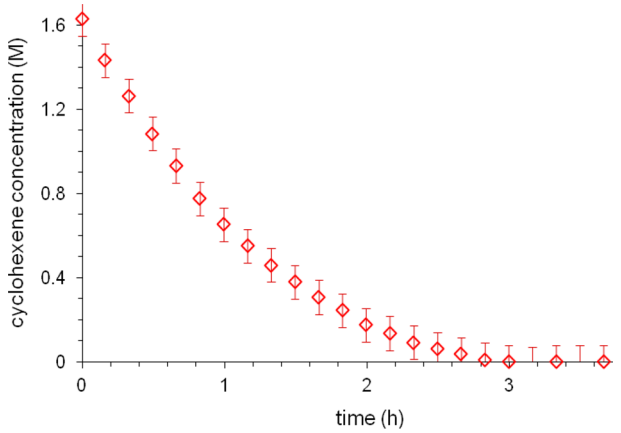

Figure 5. Kinetics characterizing the catalyst evolution as monitored by the cyclohexene hydrogenation data (◊) obtained in an experiment beginning with the fully evolved $Ir_{\sim 4-6}$/zeolite Y clusters. For clarity, only one of every 20 datum points is shown.

experimentally document the enhanced stability of $Ir_{\sim 40}$ (to ~50; vide infra) nanoparticle systems.

Moreover, DFT calculations performed by Pawluk et al.[47] predict that (naked; unligated) Ir particles prefer a rigid cubic structure until a 48-atom particle (5.91 eV per Ir atom binding energy) is reached, at which point a transition to face-centered cubic occurs. This 48-atom (about 1.1 nm diameter) limit hinders coalescence of at least naked, smaller nanoparticles because energetically unfavorable surface rearrangements would be required, again with the caveat here that these calculations refer strictly to only naked, unligated iridium nanoparticles and not those in, for example, a zeolite Y matrix such as ours. The insightful calculations by Pawluk et al. are highly consistent with and, indeed, predictive of[47] our experimental observations (op. cit.) that iridium nanoparticles in the (experimental) $Ir_{\sim 40-50}$ range exhibit a kinetics barrier to agglomeration and, therefore, have relatively high kinetic stability en route to the thermodynamic minimum of bulk $Ir(0)_n$.

Additional, Third Cycle of 3800 TTOs of Cyclohexene Hydrogenation Beginning with the Agglomerated/Sintered $Ir_{\sim 40}$ Nanoparticles: Initial Rate Plus HAADF-STEM Evidence of Further Sintering To Form $Ir_{\sim 70}$ Nanoparticles. An experiment starting with the $Ir_{\sim 40}$/zeolite Y catalyst, but a fresh 3800 equiv of cyclohexene added per mole of iridium, again yielded data characterized by immediate catalysis without any detectable induction period (Figure 7). The initial rate in this third cycle of cyclohexene hydrogenation was 0.55 M/h. Thus, these data show a further decrease in cyclohexene hydrogenation rate by 2.3 fold vs the $Ir_{\sim 4-6}$/zeolite Y catalyst and an 8.1-fold total decrease vs the initial rate characterizing the atomically dispersed Ir_1/zeolite Y catalyst. Again, the formation of larger nanoparticles was verified by the microscopic images postcatalysis. The average nanoparticle diameter had now grown to 1.30 ± 0.98 nm, corresponding, on-average, to particles approximated as $Ir_{\sim 70}$. The particle size dispersity, too, is again considerably broader, now 0.98/1.30 or 75% (Figure 8), with some particles being 2−4 fold greater in diameter than average.

Hence, both the size and the average dispersity of the iridium species increased as the agglomerative sintering progressed: from Ir_1 and ±0% size dispersion; to $Ir_{\sim 4-6}$ and 0.45 ± 0.12 (±27%) size dispersion; to $Ir_{\sim 40}$ and 1.04 ± 0.22 nm (±21%); and, finally, after the third cycle of 3800 TTOs, to $Ir_{\sim 70}$ and 1.30 ± 0.98 nm

DOI: 10.1021/acscatal.5b00321
ACS Catal. 2015, 5, 3514−3527

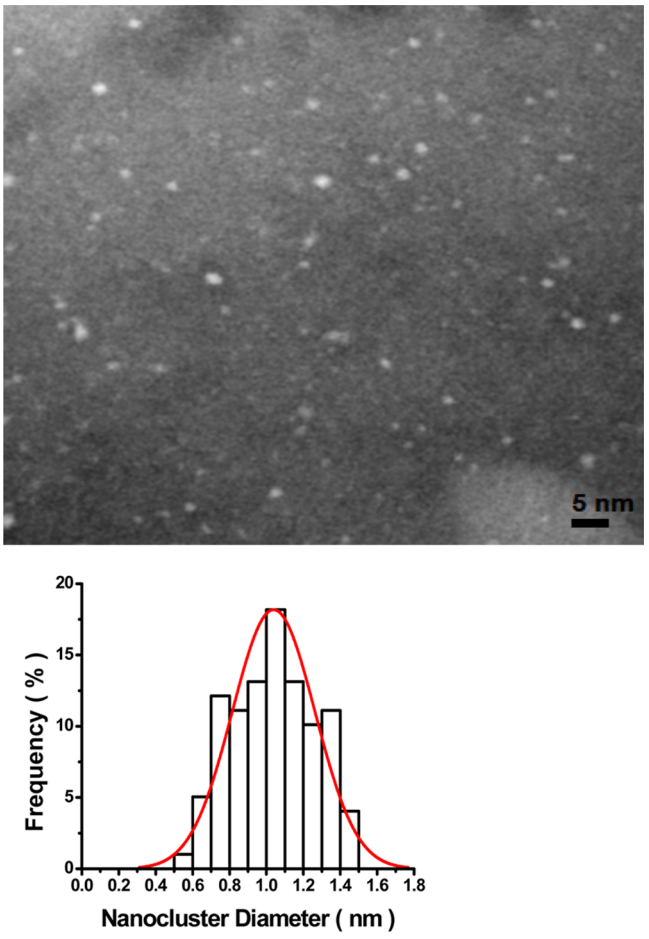

Figure 6. (top) HAADF-STEM image of the catalyst sample after the cyclohexene hydrogenation experiment, beginning with the fully evolved $Ir_{\sim 4-6}$/zeolite Y at 72.0 ± 0.1 °C and 40 ± 1 psig initial H_2 partial pressure. (bottom) Distribution of diameters measured for 98 iridium nanoparticles shown in the image at the top. The mean nanoparticle diameter was found to be 1.04 ± 0.22 nm, corresponding, on average, to $\sim Ir_{\sim 40}$.[43] The red line represents an empirical Gaussian curve-fit (OriginPro software) to the distribution of the nanocluster diameters.

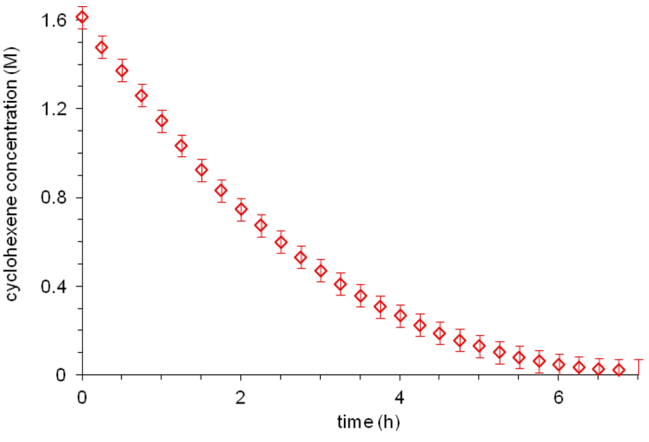

Figure 7. Kinetics of the catalyst evolution as monitored by the cyclohexene hydrogenation reporter reaction (◊) beginning, in this third cycle of 3800 TTOs, with $Ir_{\sim 40}$ nanoparticles at 72.0 ± 0.1 °C and 40 ± 1 psig initial H_2 partial pressure. For clarity, only one of every 30 datum points is shown.

(±75%). However, the data for the third cycle of catalysis and associated sintering are of special interest in that they show that a bimodal distribution of particles has formed, namely, 1.1 ± 0.2 nm (±18%) and 3.5 ± 0.9 nm (±26%), corresponding to, on-average, $Ir_{\sim 50}$ (i.e., still within error of $Ir_{\sim 40}$) and $Ir_{\sim 1600}$, respectively. Striking here is that the (experimentally) $Ir_{\sim 40-50}$ nanoparticles (i) are identical within experimental error to the Ir_{48} that the DFT calculations of Pawluk et al. predict can have enhanced stability toward agglomeration,[47] and (ii) are experimentally observed to persist even after ∼40 fold larger, $Ir_{\sim 1600}$, nanoparticles have formed. Reflection upon these results also (iii) hints at the role(s) of surface ligands formed from the reactants (cyclohexene, H_2) plus the role of the liquid cyclohexane solvent in overcoming the kinetics barrier to agglomeration of the $Ir_{\sim 40-50}$ en route to $Ir_{\sim 1600}$.

Three observations characterizing this last cycle of sintering are especially significant: (i) the (1.0 ± 0.2)-nm, $Ir_{\sim 40}$, particles are still the dominant particles present with an unchanged, ∼20%, size dispersion within experimental error; and (ii) no smaller particles are apparent in the images, as would be required if Ostwald ripening had been occurring; that is, OR is ruled out in this last cycle of sintering (and was ruled out earlier for the initial cycle of Ir_1 sintering because it is physically impossible there). The results thereby provide compelling evidence that the often-claimed OR is actually not taking place in the observed cycles of sintering of at least the present Ir_n/zeolite Y system. Moreover, (iii) the largest particles are now "explosively" (i.e., autocatalytically, vide infra) larger, $Ir_{\sim 1600}$, vs those characterizing the prior two cycles of 3800 TTOs of catalysis and associated sintering, which yielded $Ir_1 \rightarrow Ir_{4-6}$, then $Ir_{4-6} \rightarrow Ir_{\sim 40}$ particles, but the dispersion of those much larger, $Ir_{\sim 1600}$, particles is remarkably still nearly as narrow (±26%) as the $Ir_{\sim 40}$ (±20%) starting materials of this third cycle of sintering! The results demand something more insightful and specific to describe the observed sintering than the often-used words of "particle migration and coalescence." In short, and as detailed further in the Discussion section which follows, the results are consistent with and supportive of the relatively recently discovered[3−13,48,49] sintering pseudoelementary steps of autocatalytic agglomeration, which is intrinsically "explosive" (autocatalytic) in its particle size increase as well as size-narrowing, B + C → 1.5C, operating in parallel to bimolecular agglomeration, B + B → C, the primary initial step of sintering, but one that is intrinsically size-broadening.

Quantitative Curve-Fitting of the Observed Sintering Size vs Time Data, Thereby Providing Compelling Evidence for the Bimolecular and Autocatalytic Agglomeration Pseudoelementary Steps. On the basis of the previously mentioned lack of any induction period in any hydrogenation cycle, we start in what follows with "B", formally Ir(0), not A, formally Ir^I. This is not a trivial point:[50] it sets the starting point and, hence, chemical reactions, namely, B + B → C and B + C → 1.5C, as well as then the associated proper words and descriptors, specifically bimolecular agglomeration and autocatalytic agglomeration, respectively.

An important feature of the, therefore, B + B → C and B + C → 1.5C steps is that they should be able to quantitatively fit the sintering kinetics data. The fits shown in Figures 9 and 10 were accomplished with eq 1, which was derived earlier for the average diameter of the nanoparticles vs time, C, formed by the two agglomeration steps, B + B → C, and B + C → 1.5C;[49b] all reactants are treated as being "solubilized" for the purposes of the fits that follow and as detailed in the Experimental Methods and Data Analysis section. The additional assumptions or

DOI: 10.1021/acscatal.5b00321
ACS Catal. 2015, 5, 3514−3527

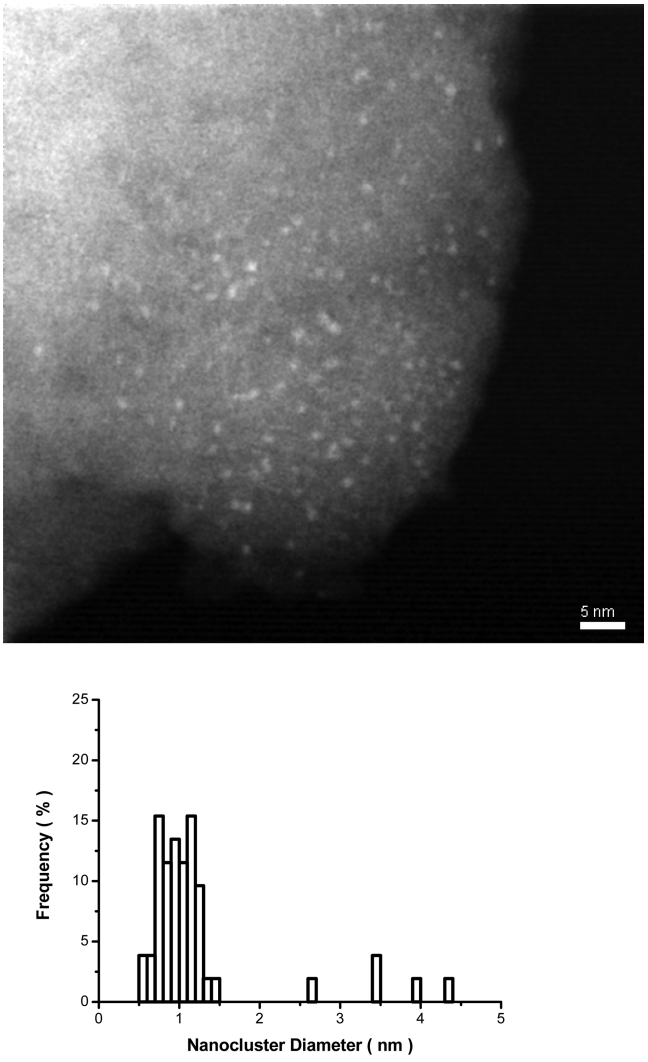

Figure 8. (top) HAADF-STEM image of the sample after the cyclohexene hydrogenation at 72.0 ± 0.1 °C and 40 ± 1 psig initial H_2 partial pressure in the experiment that began with the $Ir_{\sim 40}$/zeolite Y. (bottom) Histogram showing the iridium particle size distribution measured for the 82 particles observed in the image. The mean particle diameter was found to be 1.3 ± 0.98 nm, corresponding, on average, to $\sim Ir_{\sim 70}$ nanoparticles[43] with, as the histogram shows, a few significantly larger, ∼2.6−4.4 nm, particles. However, and more accurately, the figure reveals a bimodal distribution of particles of 1.1 ± 0.2 nm (±18%) and 3.5 ± 0.9 nm (±25%), corresponding to, on-average, $Ir_{\sim 50}$ and $Ir_{\sim 1600}$, respectively.[43]

approximations underlying the derivation and use of eq 1 are given elsewhere;[49b] the main ones to be noted for the present application of eq 1 are provided in a footnote.[51] In eq 1 the following definitions apply: D_0 and D_f are the starting and final diameters; $[B]_0$ is the starting "concentration" of Ir(0) = B; and k_3 and k_4 are the bimolecular and autocatalytic agglomeration rate constants, respectively, retaining the nomenclature and numbering for these rate constants defined in earlier publications.[48,49]

The ability of eq 1, derived from the two-step bimolecularly nucleated autocatalytic agglomeration mechanism, B + B → C, and B + C → 1.5C, to fit the observed data is obviously excellent (Figure 9). This statement seems to be especially pertinent given that no other mechanism-based equations exist that can be used to fit the data; certainly, there are no equations available from the

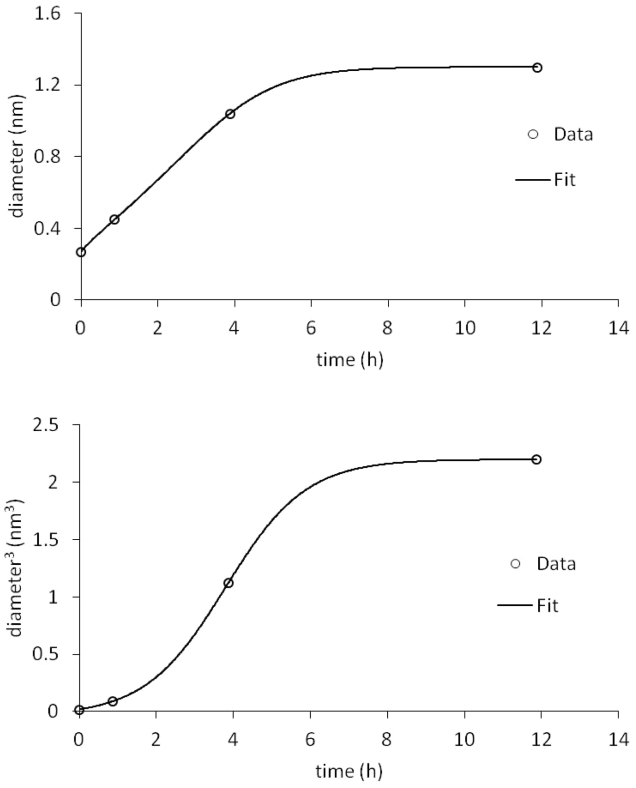

Figure 9. Fits to Ir_n diameter vs time (top) and diameter^3 vs time (bottom) assuming a final average cluster diameter of 1.3 nm (corresponding to Ir_{70}). The fits are to the "bimolecular" nucleated autocatalytic agglomeration B + B → C, B + C → 1.5C mechanism with k_3 = 28.3(3) M^{-1} s^{-1} and k_4 = 4.43(2) × 10^3 M^{-1} s^{-1} (fits were accomplished with Origin; observed residual = 9.15 × 10^{-7} nm^3).

word-only collection of phenomena known as "particle migration and coalescence."

$$D_t = \left[D_0^{\,3} + \frac{4k_3(1 - e^{k_4[B]_0 t/2})}{4k_3(1 - e^{k_4[B]_0 t/2}) - k_4}(D_f^{\,3} - D_0^{\,3}) \right]^{1/3} \quad (1)$$

Significantly, one can also fit the size vs time data if one uses the larger clusters of average diameter 3.5 nm, corresponding to, on average, $Ir_{\sim 1600}$, as the final product of the three stages of agglomeration (Figure 10).

The residual of the two fits is 4 × 10^3 times smaller (i.e., better) for the plot using $Ir_{\sim 70}$ as the average final size, an unsurprising result because $Ir_{\sim 70}$ (not $Ir_{\sim 1600}$) is, in fact, the actual, observed average diameter, eq 1 being an equation to describe the average diameter vs time. But the good fit of the progression to even the larger, 3.5 nm, $Ir_{\sim 1600}$ average diameter argues that if the third cycle of sintering had been continued until all the starting $Ir_{\sim 40}$ were consumed, then it is very likely that the two-step, "bimolecularly" nucleated, autocatalytic agglomeration mechanism would have fit those data, too.

Also noteworthy is the ability of the novel, autocatalytic, size-focusing agglomeration step, B + C → 1.5 C discovered in 2005,[48] to account for the lack of significant broadening of the size dispersion post even three cycles of agglomerative sintering. That said, the precise, empirically Gaussian form and breadth of the distribution cannot be accounted for by the two-step mechanism (which yields only an average diameter). The shape of the distribution is, therefore, an important remaining problem,

DOI: 10.1021/acscatal.5b00321
ACS Catal. 2015, 5, 3514−3527

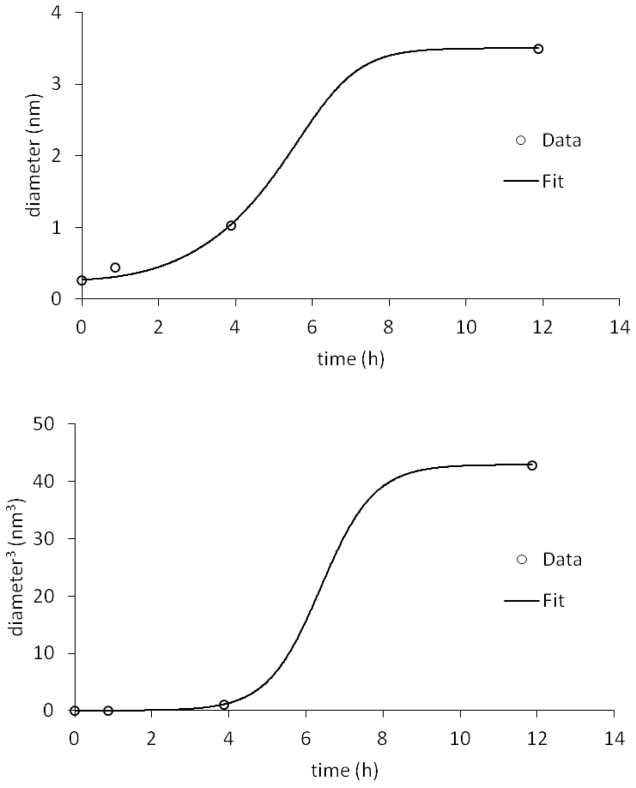

Figure 10. Fits to Ir_n diameter vs time (top) and diameter^3 vs time (bottom) assuming a final cluster diameter of the larger size of the bimodal distribution of 3.5 nm, corresponding to $Ir_{\sim 1600}$. The fits are to the autocatalytic agglomeration B + B → C, B + C → 1.5 C mechanism with $k_3 = 0.2(2)\ M^{-1}\ s^{-1}$ and $k_4 = 7(2) \times 10^3\ M^{-1}\ s^{-1}$ (using Origin; observed residual = $3.87 \times 10^{-3}\ nm^3$).

one that is currently under investigation as a separate project. Moreover, it is not clear at present whether the agglomeration happens in solution, on the zeolite support, or in both phases. Hence, those and other details of the sintering are additional important topics for future investigation.

DISCUSSION

Three Observed Stages of Sintering of an Initially Atomically Dispersed Catalyst. The results show that the initially site-isolated, mononuclear iridium complex $[Ir_1]$/zeolite Y sinters as it catalyzes cycles of 3800 turnovers of cyclohexene hydrogenation in cyclohexane solvent at 72 °C to give (a) subnanometer $Ir_{\sim 4-6}$ clusters; then (b) larger, on-average $Ir_{\sim 40}$, clusters; and further (c) even larger, approximately and on-average $Ir_{\sim 70}$ nanoparticles that are, however, better described as a bimodal distribution of, on-average, $Ir_{\sim 40-50}$ and $Ir_{\sim 1600}$ nanoparticles. Some of the nanoparticles in the $Ir_{\sim 40}$ and $Ir_{\sim 70}$ samples have diameters greater than the ∼1.3 nm diameter of the zeolite Y supercages,[52] as is evident in the images in Figures 6 and 8. It follows that the larger, ≥1.3 nm, iridium nanoparticles in these samples cannot have been encapsulated within the intact zeolite framework.

Similarly, platinum nanoparticles >1.5 nm in diameter supported on zeolite Y (formed by treatment of the supported platinum precursor in gas-phase O_2) were found to be present on external zeolite particle surfaces.[53] There is also literature evidence that growing platinum clusters/nanoparticles in zeolite X destroy the zeolite lattice as they expand.[54] All of these results support our inference that the larger, >1.3 nm, iridium nanoparticles we observed are outside the zeolite pores or present in noncrystalline zones that formed as the zeolite lattice was destroyed by the growing iridium nanoparticles. Observations by STEM of the same Ir_1 complex investigated in the present work, but in that case supported in the pores of another zeolite (HSSZ-53),[14] directly demonstrate the first steps of iridium cluster formation under the influence of the electron beam in that work.[14] The images in that study show migrating Ir atoms in the straight zeolite pores, leading to the formation of Ir_2 species, then Ir_3 species, then larger iridium nanoclusters as the zeolite framework is destroyed to create amorphous material, all further evidence consistent with the observations of the present study.

The fact that the present Ir_1/zeolite Y catalyst is stable at 22 °C, yet undergoes agglomerative sintering even under the mild conditions of 72 °C in the presence of cyclohexene, H_2, and cyclohexane, documents the well-precedented[1−12] effect of increasing temperature on catalyst sintering. In addition, whereas most reports of sintering of supported metal catalysts are concerned with samples in the presence of gas-phase reactants, our data provide a rare measure of the performance and evolution of an initially atomically dispersed catalyst in the presence of liquid-phase reactants.

Evidence Against Ostwald Ripening, but for Bimolecular and Autocatalytic Agglomeration, in the Observed Sintering. As noted in the Introduction, one of the most often cited mechanisms for sintering is Ostwald ripening, the sequence of steps of $M_n \rightarrow M_1 + M_{n-1}$, followed by M_1 migration and agglomeration with a second, larger, particle M_m, namely, $M_1 + M_m \rightarrow M_{m+1}$, in a net process $M_n + M_m \rightarrow M_{n-1} + M_{m+1}$ that, since the smaller clusters continue to "dissolve" preferentially, $M_{n-1} \rightarrow M_1 + M_{n-2}$ and so on, eventually consumes the smaller particles to make larger, lower-surface-area, particles.[14−19] We reemphasize that OR cannot physically be involved in the initial steps of sintering of our present atomically dispersed $[Ir_1]$/zeolite Y, because the putative initial OR step of $M_n \rightarrow M_1 + M_{n-1}$ leads to the nonsensical "$M_1 \rightarrow M_1$" for the case of $n = 1$. Thus, the first step of the sintering process must necessarily be the step of $Ir_1 + Ir_1 \rightarrow Ir_2$ for the present system, a rare definitive determination of a specific stoichiometry for what the literature has collected under the term "particle migration and coalescence."[3−13] Put another way, the $Ir_1 + Ir_1 \rightarrow Ir_2$ step that must be part of the sintering process is an atomic verification of the more general step of bimolecular agglomeration, B + B → C, first detailed elsewhere.[48,49]

After Ir_2 is formed, additional agglomerative sintering steps are necessary to obtain the $Ir_{\sim 4-6}$, $Ir_{\sim 40}$, and $Ir_{\sim 70}$ products observed in this investigation. Steps that include $Ir_2 + Ir_2 \rightarrow Ir_4$, $Ir_1 + Ir_2 \rightarrow Ir_3$ (the latter having been observed in the pores of HSSZ-53[14]), and so on are the expected steps, atomically precise versions of the more general steps of bimolecular agglomeration, B + B → C, and also autocatalytic agglomeration, B + C → 1.5C, where again, B represents smaller clusters or nanoparticles, and C, the larger ones.[48,49] The present work is significant in its support for the B + C → 1.5C, autocatalytic agglomeration step of catalyst particle sintering and the "explosive" size increase, yet particle-size dispersion-narrowing and, thus, size-dispersion retention properties of this new, pseudoelementary[55] step.[48,49]

A very important aspect of the two-step sintering mechanism and, hence, of the present and prior[48,49] studies, is that we now have precise chemical descriptors—bimolecular and autocatalytic agglomeration—and balanced chemical reactions—B + B → C and B + C → 1.5C—that appear to update and certainly

DOI: 10.1021/acscatal.5b00321
ACS Catal. 2015, 5, 3514−3527

make much more specific the previously word-only and, thus, chemically ill-defined collection of phenomena known as "particle migration and coalescence." That is, there are now two specific, likely more general, pseudoelementary step reactions that can serve as a foundation for particle sintering and for fitting of sintering kinetics data. These equations can and should be used in the future to test—that is, to attempt to disprove—those two steps in a given catalytic system as a now precedented sintering mechanism.

Another important aspect of the present work is that OR was also ruled out for the final step of sintering of $Ir_{\sim 40}$ because that sintering step (i) yields a bimodal distribution, yet (ii) both distributions are not defocused (not broadened) from the ~±20% size dispersity of the starting $Ir_{\sim 40}$, as would be required if OR were involved. Buhro and co-workers' studies and conclusions[56] are strongly supportive of this conclusion, specifically, their statements that (a) "Ostwald ripening is incapable of producing a bimodal distribution",[56] and (b) that OR produces "a unimodal distribution that shifts and broadens,"[56] that is, that OR is size-defocusing.[56,57] The present work therefore also reinforces the notion that particle-size distributions are key in verifying or refuting proposed sintering mechanisms.[2,6,56] In short, OR ripening can be ruled out in the initial sintering stage, starting with Ir_1, and the final sintering stage, starting with $Ir_{\sim 40}$.

Finally, we have also been able to use our data to comment on the level of "structure sensitivity" or "insensitivity" of the observed cyclohexene hydrogenation. Specifically, the initial rate plotted vs the number of accessible Ir atoms reveals that, as the clusters grow from Ir_1 to Ir_4 to $Ir_{\sim 40}$ in (or on) the zeolite Y, their catalysis of cyclohexene hydrogenation is "structure-insensitive" within a factor of 10. The data, and lead references to the extensive literature of structure-sensitive vs -insensitive reactions, are provided in the SI for the interested reader.

Issues in Need of Further Investigation. Notwithstanding the above-mentioned advances, much more remains to be learned. For example, additional investigations will be required to understand better which factors are important in the sintering of initially atomically dispersed metals in contact with liquids, including (i) the presence of ligands such as H (i.e., metal hydrides) or olefins, such as cyclohexene; and, as already noted, (ii) the liquid medium, which may ligate and solvate species (especially the smallest ones) and enable recently precedented off-the-support, solution-based mechanisms for the enhanced mobility and resultant sintering of initially supported catalysts.[58] Furthermore, (iii) in-operando SAXS studies of homogeneous systems that can track both the size distribution and number of particles promise to provide insight.[2,6,56] In the future, it will also likely prove important to (iv) tie in studies, such as the present one, concerned with sintering species in contact with a liquid phase, to studies of sintering of gas−solid-phase systems. A section has been added to the SI, entitled "Sintering of Ir_1/HY Zeolite in the Presence of Gas-Phase Reactants: Evidence for the Chemistry in the First Steps of Sintering", with this important future goal in mind.

Also worth mentioning is the well-established precedent for faster sintering of metals under the influence of ligands, exemplified by the effects of CO on the sintering of Pd_n.[25] These results are contrasted with the effects of CO ligands on mononuclear iridium complexes on our support—which inhibit the first steps of sintering by inhibiting iridium hydride formation.[15] We also recognize that the interactions of liquids with supports may be substantially different from interactions of gases with supports and that changes in the supports during sintering can affect the sintering processes, especially when the metal species are very small. The liquid environment might affect the sintering process more after the nanoparticles have grown so large as to destroy the zeolite lattice and been freed from its constraints. Correspondingly, we do not rule out the possibility that more than one "mechanism" of sintering might have been in play. Nonetheless, we emphasize that—at a minimum—a mechanism of the bimolecular and autocatalytic agglomeration steps accounts quantitatively for our average size vs time sintering kinetics data.

CONCLUSIONS

The present work is an examination of an atomically dispersed, well-defined $[Ir(C_2H_4)_2]$/zeolite Y precatalyst under three successive cycles of 3800 TTOs of cyclohexene hydrogenation, 11 400 TTOs of catalysis. The evolution of the resultant catalyst has been followed by measuring the initial rate of catalysis at the start of each cycle and then characterizing the products by EXAFS spectroscopy and HAADF-STEM. The main findings are summarized as follows:

- Overall, the present work comprises the first investigation of the sequential agglomerative sintering of a well-defined, atomically dispersed, supported catalyst as it undergoes a series of catalytic cycles in contact with liquid-phase reactants (cyclohexene, H_2) and solvent (cyclohexane).
- A sequence of agglomerative sintering was observed for samples on-average of Ir_1 to $Ir_{\sim 4-6}$ to $Ir_{\sim 40}$ to $Ir_{\sim 70}$ as they went through successive cycles of 3800 TTOs of cyclohexene hydrogenation, the final size distribution being more accurately described as a bimodal distribution of, on-average, $Ir_{\sim 40-50}$ and $Ir_{\sim 1600}$ particles. The atomically dispersed Ir_1/zeolite Y, which was stable during cyclohexene hydrogenation catalysis at 22 °C,[31] is, however, not stable at the only 50 °C higher temperature of 72 °C in the presence of H_2 and liquid cyclohexene substrate and cyclohexane solvent.
- Because the initial iridium species was atomically dispersed, Ir_1, the first stages of aggregation cannot involve Ostwald ripening as its initial step (for $n = 1$) of $M_n \rightarrow M_1 + M_{n-1}$. The present sintering data therefore represent the simplest and most fundamental case of metal aggregation, namely, that involving migration of the metal through the pores of zeolite Y and the resultant Ir−Ir bond formation. The results are also of significance in that no evidence for, and instead compelling evidence against, Ostwald ripening was obtained for the final stage of sintering starting from $Ir_{\sim 40}$.
- The results complement and expand those presented previously[14,15] in which the initial stage of aggregation of iridium beginning with the $[Ir(C_2H_4)_2]$/zeolite precatalyst is triggered by reduction of the iridium by H_2 (leading to iridium hydride formation) but, in that case, via gas-phase reactants. The present data, instead, demonstrate sintering of an initially atomically dispersed, supported catalyst in the presence of liquid-phase reactants. However, the task of integrating the present solution-phase sintering studies with prior gas-phase studies remains.
- Our results document the enhanced kinetics stability toward agglomeration of supported $Ir_{\sim 40-50}$ clusters, consistent with our other work on $Ir_{\sim 40}$ clusters[46] stabilized by $AlEt_3$. Our results are also highly supportive of the DFT calculations by Pawluk et al.[47] predicting that

DOI: 10.1021/acscatal.5b00321
ACS Catal. 2015, 5, 3514−3527

Ir_{48} clusters are stabilized by a rearrangement barrier from their cubic-closed packed structure to a fcc structure.

- The results also bear heavily on the concept of atomically dispersed catalysts.[31] In particular, our results document that true, stable, atomically dispersed, sinter-resistant catalysts promise to be challenging to prepare and will require documentation of their sinter-resistance, especially when in contact with liquid reagents and ligands such as olefins, CO,[25] and others, especially those such as H_2 that reduce the metal. That said, there are notable examples of highly sinter-resistant, atomically dispersed catalysts with metals in nonzero oxidation states, a notable recent example being an Fe/SiO_2 catalyst in which the iron is embedded in a silica matrix post a synthesis that involves 1973 K and molten silica as part of the catalyst preparation.[59] Such catalysts typically involve metals that are oxophilic.
- Significantly, the sintering average size vs time data starting from the atomically dispersed catalyst were quantitatively accounted for by the two-step sintering mechanism of B + B → C and B + C → 1.5C, an unprecedented result.
- An important finding from the present investigation is the definitive evidence against OR at the initial and final stages of the sintering along with evidence of the pseudoelementary-step sintering steps, of bimolecular and autocatalytic agglomeration, B + B → C and B + C → 1.5C. The data also fortify the expectation[48,49] that the novel, autocatalytic agglomeration step can lead to explosive particle growth while largely maintaining the particle size distribution via the intrinsic particle-size focusing nature of this novel[48,49] step. Both of these specific, balanced chemical reactions provide the proper, more specific, words to describe catalyst sintering, as well as specific chemical equations that can be used to fit sintering kinetics data and thereby test quantitatively proposed sintering mechanisms. In that way, an important step has been accomplished beyond the word-only statement that is a collection of phenomena, but not a chemical mechanism, for sintering known as "particle migration and coalescence."
- We recognize that important questions remain, including but not limited to the following: (a) the role of liquid in the sintering process; and (b) whether the nature of the sintering, perhaps influenced by the liquid, is essentially different when the confining role of the zeolite pores is removed.

EXPERIMENTAL METHODS AND DATA ANALYSIS

Materials and General Considerations. *Sample Syntheses at UCD.* Sample syntheses and handling were performed with the exclusion of moisture and air. The highly dealuminated HY zeolite (DAY zeolite) (Zeolyst International, CBV760), with a Si/Al atomic ratio of ∼30, was calcined in O_2 at 500 °C for 4 h and evacuated for 16 h at 500 °C. After calcination, the zeolite powder was isolated and stored in an argon-filled drybox (MBraun, with an H_2O concentration <0.5 ppm and an O_2 concentration <5 ppm, as monitored by VAC monitors equipped with LM-H_2O-A and LM-O_2-A alarms). *n*-Pentane (Fisher, 99%) was dried and purified by column chromatography (Grubbs apparatus, MBraun SPS) in the presence of argon.

Cyclohexene Hydrogenation Experiments at CSU. Unless indicated otherwise, all manipulations were performed under N_2 in a Vacuum Atmospheres drybox. Oxygen concentrations were continuously maintained in the drybox at ≤5 ppm, monitored by a Vacuum Atmospheres O_2 monitor. Unless noted otherwise, all solvents, compounds, and other materials mentioned below were stored in the drybox. Cyclohexane (99.5%, anhydrous, Aldrich) was used as received. Cyclohexene (99%, inhibitor free) was distilled over sodium metal under argon. H_2 was purchased from General Air (>99.5%) and passed through a Trigon Moisture Trap and a Trigon Technologies Oxygen/Moisture Trap to remove O_2 and H_2O, followed by a Trigon Technologies High Capacity Indicating Oxygen Trap. The conversion of cyclohexene to cyclohexane was verified by recording a ^1H NMR spectrum of a sample prepared by adding a drop of the resultant product solution into 1 mL of CD_2Cl_2 (Cambridge Isotope Laboratories) on a Varian INOVA-300 instrument, 300.115 MHz for ^1H (cyclohexene: 5.5 ppm (m), 2 ppm (m), 1.6 ppm (m); cyclohexane: 1.4 ppm (s)).

Sample Transport Between UCD and CSU. The samples to be shipped to either CSU (for cyclohexene hydrogenation experiments) or to UCD (for characterization by HAADF-STEM and for preparation for transport to a synchrotron for EXAFS spectroscopy), were prepared in the drybox. The samples were placed into a stainless-steel vacuum tube, the ends were clamped together and sealed with O-rings, and the samples were then shipped to the other laboratory or to the synchrotron, where the vacuum tube was opened in a drybox and prepared for the reactions or analyses. The exclusion of air/O_2 was meticulously maintained by careful handling and preparing the samples under N_2 in a Vacuum Atmospheres drybox for the cyclohexene hydrogenation experiments at CSU and the EXAFS and HAADF-STEM analyses at UCD or at the synchrotron.

Catalytic Hydrogenation Apparatus. All the hydrogenation reactions were carried out with the previously described, custom-built pressurized hydrogenation apparatus that allows monitoring of the H_2 pressure loss in real time with a precision of ±0.01 psig via a PC interface (LabView ver. 8.2).[60,61] A Fischer-Porter (F-P) bottle was connected via its Swagelok TFE-sealed Quick Connect fittings to a hydrogenation line and an Omega D1512 10 V A/D converter with an RS-232 connection to a PC. Post monitoring of the H_2 uptake data via the computer interface, the data were converted to cyclohexene consumption using the known 1:1 H_2/cyclohexene stoichiometry,[32] then the cyclohexene hydrogenation data were corrected for the cyclohexene plus cyclohexane solution vapor pressure by using the previously established protocol.[32] Specifically, the cyclohexene plus cyclohexane solution vapor pressure was measured independently, and a point-by-point subtraction from the raw H_2 uptake data was applied to the cyclohexene hydrogenation data in Figures 2, 5, and 7 (see the Supporting Information for independent cyclohexene plus cyclohexane solution vapor pressure measurements and the point-by-point subtraction correction).

Each of the cyclohexene hydrogenation datum points presented here was repeated at least three times, yielding the same result within ±10% error; the reproducibility tests included experiments with independently prepared catalyst samples.

Initial Rate Determinations. The initial rates were determined by polynomial fitting of the cyclohexene loss vs time data to a third-order polynomial. The derivative of this polynomial at $t = 0$ yields the initial rate.[62]

Synthesis and Characterization of $[Ir(C_2H_4)_2]$/Zeolite Y Containing 1 wt % Iridium. $[Ir(C_2H_4)_2(acac)]$ (acac = $CH_3COCH_2COCH_3$) was synthesized and characterized as described elsewhere[63] and slurried in dried *n*-pentane at ice

DOI: 10.1021/acscatal.5b00321
ACS Catal. 2015, 5, 3514−3527

temperature with the calcined zeolite powder in a Schlenk flask. The stirred slurry was warmed to room temperature, and after 1 day, the solvent was removed by evacuation for a day. The resultant solid, $[Ir(C_2H_4)_2]$/zeolite Y, containing 1 wt % iridium, was characterized[31] by EXAFS, IR, and NMR spectroscopies and stored in the argon-filled drybox.

Procedure for Cyclohexene Hydrogenation Reaction under Standard Conditions Starting with $[Ir(C_2H_4)_2]$/Zeolite Y. To begin, 25 (±1) mg of $[Ir(C_2H_4)_2]$/zeolite-Y (1 wt % Ir) (1.3 μmol Ir) was weighed in a 2-dram glass vial and then transferred into a new 22 × 175 mm Pyrex culture tube containing a new 5/16 × 5/8-in. Teflon-coated stir bar. Cyclohexane (2.5 mL) and cyclohexene (0.5 mL, 4.94 mmol) were added via separate gastight syringes. The culture tube was sealed inside the F-P pressure bottle and brought outside the drybox. The F-P bottle was immersed into the oil bath until the top level of solution in the culture tube was the same as the level of the oil. The upper part of the F-P bottle was insulated from the lower hot part with an insulator tape and cooled by blowing cooler, room-temperature air across the F-P bottle using a heat gun in the blower (not heat) mode mounted on a ring-stand. The specific placement, tape-insulating, and cooling of the (non-immersed parts) of the F-P bottle are essential to the success and reproducibility of the hydrogenations, being necessary to avoid the vaporization and condensation of volatiles outside the culture tube placed inside the F-P bottle and to avoid artifactual induction periods, all while keeping the immersed part of the F-P bottle and reaction system at 72.0 ± 0.1 °C for days. The oil bath was held at a constant-temperature using a circulating bath at 72.0 ± 0.1 °C. The F-P bottle was connected via Swagelok TFE-sealed Quick-Connects to the hydrogenation line, which was pre-evacuated for at least 30 min to remove any traces of oxygen and water. The solution in the culture tube was stirred at 600 rpm for 5 min so that the solution temperature reached 72 °C before filling with purified H_2 at 40 ± 1 psig (~2.7 atm). The F-P bottle was then purged 10 times with H_2 (5 s per purge), and the reaction was started at time $t = 0$.

When the H_2 uptake ceased (as observed via the PC interface and ^{1}H NMR spectroscopy), the F-P bottle was disconnected from the hydrogenation line, the remaining H_2 pressure was released, the F-P bottle was transferred back into the drybox, and the resultant sample in the culture tube was transferred into a new 20 mL scintillation vial with a new 5/16 × 5/8-in. Teflon-coated stir bar and dried under vacuum for 8 h. This sample was sealed in a stainless steel vacuum tube, brought out of the drybox, and shipped to UCD for characterization studies.

The standard conditions cyclohexene hydrogenation reaction experiment starting with the $[Ir(C_2H_4)_2]$/zeolite Y precatalyst was repeated 10 times, yielding the same result within ±5% error in the initial reaction rate.

Cyclohexene Hydrogenation with the Fully Evolved $Ir_{\sim 4-6}$/Zeolite Y and $Ir_{\sim 40}$/Zeolite Y Clusters. The cyclohexene hydrogenation reaction under the standard conditions starting with $[Ir(C_2H_4)_2]$/zeolite Y was repeated at 72.0 ± 0.1 °C, with one variation: the reaction mixture was kept in the line at 72 °C for ~2 days under the remaining H_2 pressure[36] (~25 psig) to allow a complete evolution of the zeolite-supported $Ir_{\sim 4-6}$ clusters. Next, the F-P bottle was removed from the line and, after release of the residual hydrogen pressure, taken into the drybox, where 0.5 mL of fresh cyclohexene was added in less than 1 min, giving a solution of 3 mL of cyclohexane plus 0.5 mL of cyclohexene. The F-P bottle was then resealed, taken out of the drybox, and immersed into the oil bath until the top level of the solution in the culture tube was the same as the level of the oil, as previously described. The upper part of the F-P bottle was insulated from the lower hot part with an insulator tape and cooled by blowing cool air (vide supra). The solution in the culture tube was stirred at 600 rpm for 5 min so that the solution reached a temperature of 72 °C before being filled with purified H_2 at 40 ± 1 psig (~2.7 atm). The F-P bottle was then reconnected to the hydrogenation line and purged 10 times with H_2 (5 s per purge), and the cyclohexene hydrogenation reaction was started at $t = 0$.

The subsequent cyclohexene hydrogenation reaction was also performed beginning with the sample resulting from the above procedure by removing the F-P bottle from the line when the cyclohexene hydrogenation ceased (~4 h via PC interface and ^{1}H NMR spectroscopy). Then the F-P bottle was vented and taken into the drybox, where 0.5 mL of fresh cyclohexene was quickly added in less than 1 min; resealed; taken out of the drybox; reconnected to the hydrogenation line in the same way as described above; and stirred at 600 rpm for 5 min so that the solution reached a temperature of 72 °C before being filled with purified H_2 at 40 ± 1 psig (~2.7 atm). The F-P bottle was then purged 10 times with H_2 (5 s per purge), and the third cycle of cyclohexene hydrogenation was started.

In separate experiments, when the H_2 uptake ceased (as observed via the PC interface and ^{1}H NMR spectroscopy) for all runs, the F-P bottle was disconnected from the hydrogenation line, the remaining H_2 pressure was released, the F-P bottle was transferred back into the drybox, and the resulting product in the culture tube was transferred into a new 20 mL scintillation vial with a new 5/16 × 5/8-in. Teflon-coated stir bar and dried under vacuum for 8 h. These samples were sealed in a stainless steel vacuum tube, brought out of the drybox, and shipped to UCD for characterization studies.

Kinetics Fitting of the D and D^3 Average Size vs Time Data. The average diameter (D) vs time data from the three cycles of sintering was fit using eq 1 (vide supra), as follows: An initial single Ir atom in the Ir_1/zeolite HY sample, with its atomic diameter of 0.272 nm, was used as the starting "cluster". The times for the three data points past $t = 0$ were obtained by adding the times from each experiment, judging each of the three catalytic hydrogenation and sintering cycles to be complete once the cyclohexene concentration had run below 0.01 M (hence, the first run was judged complete after 0.87 h; the second run, after 3.00 h; and the third run, after 8.00 h, so that the total time was 11.87 h). The ~48 h during which the Ir_{4-6} clusters were allowed to form was not added; including this time decreased the quality of the fits (see the Supporting Information for those fits). The initial concentration of Ir, $[B]_0$, in the fits to eq 1 was determined from the initial reaction solution containing 25 mg of $[Ir(C_2H_4)_2]$/zeolite Y (1 wt % Ir), corresponding to 0.25 mg of Ir, or 1.3×10^{-6} mol. In the initial solution of 2.5 mL cyclohexane and 0.5 mL cyclohexene, in turn, gives this an initial Ir concentration, or $[B]_0$, of 4.3×10^{-4} M. That is, the Ir/zeolite Y catalyst was regarded as "solubilized" for the purposes of fitting the diameter vs time data. The volume increase was 0.5 mL (resulting from the addition of a fresh 0.5 mL of cyclohexene) in each sintering cycle (i.e., and over and above the initial volume of 3.0 mL) so that the concentration of sintering particles was decreasing by ~14%, 25%, and 34% in the three sintering cycles. This effect has been neglected in the fits, since simulations show that such a correction is not expected to have significant effects on the quality of the fits (see the Supporting Information for the simulations). The reported bimolecular rate constants will be

DOI: 10.1021/acscatal.5b00321
ACS Catal. 2015, 5, 3514−3527

increasingly too small by, on average, approximately the squares of these percentage values, but they could be corrected for this dilution effect if others use our rate constants and want more precise values.

X-ray Absorption Spectroscopy. The X-ray absorption spectra were recorded at X-ray beamline X18-B of the National Synchrotron Light Source (NSLS) at Brookhaven National Laboratory (BNL) and at beamline 4-1 of the Stanford Synchrotron Radiation Lightsource (SSRL). The storage ring electron energy and ring current were ~3 GeV and 200−300 mA, respectively. Si(111) and Si(220) double-crystal monochromators were used at BNL and SSRL, respectively. Each monochromator was detuned to 80% of maximum intensity to reduce the interference of higher harmonics in the X-ray beam.

To minimize the exposure to air and moisture, each powder sample was placed in a glass vial and sealed with Parafilm inside the argon-filled drybox. Each glass vial was placed into a stainless-steel Swagelok vacuum tube sealed with O-rings for transfer to the synchrotron. The mass of each sample (~0.3 g) was chosen to give an absorbance between 1.5 and 3.0 calculated at 50 eV above the Ir L_{III} edge (11215 eV). In an N_2-filled glovebox at the synchrotron, each sample was pressed into a wafer and mounted in a cell for transmission spectroscopy[64] and maintained under vacuum (at a pressure of 10^{-7} kPa) at liquid-nitrogen temperature during the data collection. X-ray intensity data were collected in transmission mode by use of ion chambers mounted on each end of the sample cell.

EXAFS Data Analysis. The X-ray absorption edge energy was calibrated with the measured signal of a platinum foil (scanned simultaneously with the sample) at the Pt L_{III} edge, which was taken to be the inflection point at 11564 eV. The data were normalized by dividing the absorption intensity by the height of the absorption edge.

Analysis of the EXAFS data was carried out with the software ATHENA of the IFEFFIT[65,66] package and the software XDAP developed by Vaarkamp et al.[67] Each spectrum that was analyzed was the average of four spectra. ATHENA was used for edge calibration and deglitching. XDAP was used for background removal, normalization, and conversion of the data into an EXAFS (χ) file. A "difference-file" technique for shell isolation was applied with XDAP for determination of optimized fit parameters. A second-order polynomial was fit to the data in the pre-edge region and subtracted from the entire spectrum in each analysis. The functional that was minimized and the function used to model the data are reported elsewhere.[68] The background was subtracted by using cubic spline routines. Reference backscattering phase shifts were calculated with the software FEFF7[69] from crystallographic data. $Ir(C_2H_4)_2(acac)$[63] was used as the reference for $Ir-O_{support}$, Ir−C, $Ir-O_{long}$, and $Ir-C_{long}$ (the latter two being Ir−O and Ir−C contributions at distances longer than bonding distances); Ir−Al alloy[70] was used for Ir−Al contributions, and iridium metal was used for Ir−Ir first- and second-shell contributions. Iterative fitting was done in R (distance) space with the Fourier-transformed χ data until optimum agreement was attained between the calculated k^0-, k^1-, k^2-, and k^3-weighted EXAFS data and each postulated model (k is the wave vector). The number of parameters used in the fitting was always less than the statistically justified number, computed with the Nyquist theorem:[71] $n = (2\Delta k \Delta r/\pi) + 1$, where Δk and Δr are the k and r ranges used in the fitting, respectively, and r is the interatomic absorber−backscatterer distance.

For each analysis of EXAFS data characterizing each sample, several candidate models were investigated that were selected on the basis of the expected and plausible contributions. See the Supporting Information for the analysis of those models for each sample. We emphasize that attempts were made to include Ir−Ir contributions in each model to test for the presence/absence of iridium clusters. Each candidate model was compared with the data and evaluated on the basis of the goodness of fit for each individual shell and for the data overall. The estimated errors in the reported coordination numbers and bond distances are ±20% and ±0.02 Å, respectively.

HAADF-STEM: Sample Handling, Instrumentation, and Analysis. To minimize the exposure to air and moisture, powder samples (shipped from CSU) were loaded onto a lacey carbon, 300-mesh copper grid (Ted-Pella) in the argon-filled drybox. The grid was packed in an Eppendorf tube and sealed with Parafilm inside the drybox. Each Eppendorf tube was placed into a stainless-steel Swagelok vacuum tube sealed with O-rings for transfer to the microscope facility, where an argon-filled glovebag (Glas-Col) was purged five times with ultrahigh-purity argon (Praxair, grade 5.0), and the TEM grid was loaded onto the TEM holder under a blanket of flowing argon in the glovebag. The TEM holder was then inserted into the microscope under flowing argon, with a time of possible exposure to air of <5 s.

Prior to imaging of a sample, the aberration corrector was aligned with a Pt/Ir-on-holey-carbon standard sample (SPI Supplies) until atomic resolution of the metal particles was achieved and the lattice spacings of the metals were confirmed.

Images of the samples were obtained with a JEOL JEM-2100F electron microscope. The microscope was equipped with a field emission gun (FEG), operating at 200 kV, with a CEOS hexapole probe (STEM) aberration corrector. The images were captured by an HAADF detector with a collection semiangle of 75−200 mrad and a probe convergence semiangle of 17.1 mrad. To minimize artifacts in the images caused by beam damage, the microscope was aligned for one region of the sample, and then the beam was shifted to a neighboring region for a quick image acquisition: 5 s for a 512 × 512 pixel size.

HAADF-STEM Image Size Analysis. For each cluster/nanoparticle, an intensity profile was obtained by using the Digital Micrograph software (Gatan). Line profiles were then transferred to OriginPro for baseline correction. Background-subtracted profiles of the clusters were fitted to a Gaussian distribution function in OriginPro, and full-width-half-maximum (fwhm) values of the fitted peak were reported as the diameter of each iridium cluster metal framework.

■ ASSOCIATED CONTENT

Supporting Information

The Supporting Information is available free of charge on the ACS Publications website at DOI: 10.1021/acscatal.5b00321.

Details of EXAFS data analysis and methods for selection of best-fit models; vapor pressure corrections by point-by-point subtraction of cyclohexene plus cyclohexane vapor pressure from hydrogenation raw kinetics data; a discussion of literature analysis of sintering kinetics data via empirical power-laws; a section titled "Including the ~48 Hours Under H_2 in the Data, Then Curve-fitting the Resultant Ir_n Size vs. Time Data"; a section titled "Fitting Simulated Size vs. Time Data to Examine the Effect of Changing Cluster Concentration"; a section titled "Sintering of Ir_1/HY Zeolite in the Presence of Gas-Phase Reactants: Evidence for the Chemistry in the First Steps of Sintering"; and a section titled "The Relative Rate

DOI: 10.1021/acscatal.5b00321
ACS Catal. 2015, 5, 3514−3527

and Degree of 'Structure Insensitivity' of the Catalytic Cyclohexene Hydrogenation Over the Range of Metal Species Examined" (PDF)

AUTHOR INFORMATION

Corresponding Authors

*E-mail: bcgates@ucdavis.edu.
*E-mail: rfinke@lamar.colostate.edu.

Present Address

⊥(E.B.) Shoei Electronic Materials, Inc. 1110 NE Circle Blvd. Corvallis, OR 97330 USA.

Notes

The authors declare no competing financial interest.

ACKNOWLEDGMENTS

The research at Colorado State University and the University of California was supported by the Department of Energy (DOE), Basic Energy Sciences Grants DE-FG02-03ER15453 (at CSU), DE-SC005822 (JL), and DE-FG02-03ER46057 (CA) (at UCD). We thank the DOE Division of Materials Sciences for its role in the operation and development of beamline 4-1 at the Stanford Synchrotron Radiation Lightsource and beamline X-18B at the National Synchrotron Lightsource. We thank the beamline staffs for valuable support.

REFERENCES

(1) Supported catalyst sintering is widely believed to occur via two generic mechanisms: (i) Ostwald ripening (OR), and (ii) the collection of pheonomena known as particle migration and coalescence (PMC). OR proceeds via the migration/diffusion of atoms,[2] whereas PMC is believed to proceed, as the name implies, via the migration/diffusion of intact catalyst particles.[3,4] No consensus exists regarding which mechanism(s) operate(s) under a given set of conditions, and the possibility that both processes may occur simultaneously[3] is often overlooked. See the Supporting Information for a brief discussion of literature analyses of sintering kinetics data via empirical power laws.

(2) For TEM investigations of sintering, in which Ostwald ripening processes are proposed, see: Simonsen, S. B.; Chorkendorff, I.; Dahl, S.; Skoglundh, M.; Sehested, J.; Helveg, S. *J. Am. Chem. Soc.* **2010**, *132*, 7968−7975.

(3) Bartholomew, C. H. *Appl. Catal., A* **2001**, *212*, 17−60.

(4) Moulijn, J. A.; van Diepen, A. E.; Kapteijn, F. In *Handbook of Heterogeneous Catalysis*, 2nd ed.; Ertl, G., Knözinger, H., Schüth, F., Weitkamp, J., Eds.; Wiley-VCH: Weinheim, 2008.

(5) Bartholomew, C. H.; Farrauto, R. J. *Fundamentals of Industrial Catalytic Processes*, 2nd ed.; Wiley: Hoboken, NJ, 2006.

(6) For nanoplasmonic spectroscopy studies of sintering, in which Ostwald ripening is proposed as the main sintering mechanism, see: Larsson, E. M.; Millet, J.; Gustafsson, S.; Skoglundh, M.; Zhdanov, V. P.; Langhammer, C. *ACS Catal.* **2012**, *2*, 238−245.

(7) Bartholomew, C. H. *Kirk-Othmer Encyclopedia of Chemical Technology*; Wiley: New York, 2003; Vol. *5*; p 255.

(8) For investigations of sintering involving model catalysts performed with single-crystal and high-vacuum systems, see, for example: (a) Campbell, C. T. *Acc. Chem. Res.* **2013**, *46*, 1712−1719. (b) Parker, S. C.; Campbell, C. T. *Top. Catal.* **2007**, *44*, 3−13. (c) Campbell, C. T.; Parker, S. C.; Starr, D. E. *Science* **2002**, *298*, 811−814. (d) Yang, S.; Qiu, P.; Yang, G. *Carbon* **2014**, *77*, 1123−1131. (e) Liu, H.; Zhang, L.; Wang, N.; Su, D. S. *Angew. Chem., Int. Ed.* **2014**, *53*, 12634−12638. (f) Moonen, P. F.; Bat, E.; Voorthuijzen, W. P.; Huskens, J. *RSC Adv.* **2013**, *3*, 18498−18505. (g) Yoon, K.; Yang, Y.; Lu, P.; Wan, D. H.; Peng, H. C.; Masias, K. S.; Fanson, P. T.; Campbell, C. T.; Xia, Y. N. *Angew. Chem., Int. Ed.* **2012**, *51*, 9543−9546.

(9) (a) Datye, A. K.; Xu, Q.; Kharas, K. C.; McCarty, J. M. *Catal. Today* **2006**, *111*, 59−67. (b) Hansen, T. W.; DeLaRiva, A. T.; Challa, S. R.; Datye, A. K. *Acc. Chem. Res.* **2013**, *46*, 1720−1730. (c) DeLaRiva, A. T.; Hansen, T. W.; Challa, S. R.; Datye, A. K. *J. Catal.* **2013**, *308*, 291−305. (d) Xu, Q.; Kharas, K. C.; Croley, B. J.; Datye, A. K. *Top. Catal.* **2012**, *55*, 78−83.

(10) See, for example: (a) Bartholomew, C. H. *Appl. Catal., A* **1993**, *107*, 1−57. (b) Lee, H. H. *J. Catal.* **1980**, *63*, 129−137. (c) Stassinos, E. C.; Lee, H. H. *Chem. Eng. Sci.* **1995**, *50*, 1337−1345. (d) Manninger, I. *J. Catal.* **1984**, *89*, 164−167. (e) Fuentes, G. A. *Appl. Catal.* **1985**, *15*, 33−40. (f) Fuentes, G. A.; Salinas-Rodriguez, E. *Stud. Surf. Sci. Catal.* **2001**, *139*, 503−510.

(11) Bartholomew, C. H. *Stud. Surf. Sci. Catal.* **1997**, *111*, 585−592.

(12) Spivey, J. J.; Agarwal, S. K.; Bartholomew, C. H. *Catalysis* **1993**, *10*, 41−82.

(13) Zhai, Y.; Pierre, D.; Si, R.; Deng, W.; Ferrin, P.; Nilekar, A. U.; Peng, G.; Herron, J. A.; Bell, D. C.; Saltsburg, H.; Mavrikakis, M.; Flytzani-Stephanopoulos, M. *Science* **2010**, *329*, 1633−1636.

(14) Aydin, C.; Lu, J.; Liang, A. J.; Chen, C.-Y.; Browning, N. D.; Gates, B. C. *Nano Lett.* **2011**, *11*, 5537−5541.

(15) Lu, J.; Aydin, C.; Browning, N. D.; Gates, B. C. *J. Am. Chem. Soc.* **2012**, *134*, 5022−5025.

(16) Ratnasamy, P.; Srinivas, D.; Knözinger, H. *Adv. Catal.* **2004**, *48*, 1−169.

(17) Uzun, A.; Gates, B. C. *J. Am. Chem. Soc.* **2009**, *131*, 15887−15894.

(18) Noteworthy here is that, although they were determined ex situ, the data reported both here and elsewhere[31] strongly argue that the EXAFS and HAADF-STEM data accurately report on the aggregation state, *n*, of at least the present Ir_n/zeolite Y catalysts without introducing artifacts. Specifically, our ability to consistently image and characterize atomically dispersed iridium in Ir_1/zeolite Y (when present) argues compellingly against at least significant agglomeration induced by either the EXAFS or HAADF-STEM measurements and for this relatively refractory, metal system with its relatively strong, third-row metal, Ir−Ir and Ir−support bonds.

(19) Uzun, A.; Dixon, D. A.; Gates, B. C. *ChemCatChem* **2011**, *3*, 95−107.

(20) Xu, Z.; Xiao, F.-S.; Purnell, S. K.; Alexeev, O.; Kawi, S.; Deutsch, S. E.; Gates, B. C. *Nature* **1994**, *372*, 346−348.

(21) Argo, A. M.; Odzak, J. F.; Lai, F. S.; Gates, B. C. *Nature* **2002**, *415*, 623−626.

(22) Yang, X.-F.; Wang, A.; Qiao, B.; Li, J.; Liu, J.; Zhang, T. *Acc. Chem. Res.* **2013**, *46*, 1740−1748.

(23) (a) Schüth, F. *Angew. Chem., Int. Ed.* **2014**, *53*, 8599−8604. (b) Cao, X.; Ji, Y.; Luo, Y. *J. Phys. Chem. C* **2015**, *119*, 1016−1023. (c) Li, F.; Li, Y.; Zeng, X. C.; Chen, Z. *ACS Catal.* **2015**, *5*, 544−552.

(24) Flytzani-Stephanopoulos, M.; Gates, B. C. *Annu. Rev. Chem. Biomol. Eng.* **2012**, *3*, 545−574.

(25) Parkinson, G. S.; Novotny, Z.; Argentero, G.; Schmid, M.; Pavelec, J.; Kosak, R.; Blaha, P.; Diebold, U. *Nat. Mater.* **2013**, *12*, 724−728.

(26) Kyriakou, G.; Boucher, M. B.; April, D.; Jewell, A. D.; Lewis, E. A.; Lawton, T. J.; Baber, A. E.; Tierney, H. L.; Flytzani-Stephanopoulos, M.; Sykes, E. C. H. *Science* **2012**, *335*, 1209−1212.

(27) Qiao, B.; Wang, A.; Yang, X.; Allard, L. F.; Jiang, Z.; Cui, Y.; Liu, J.; Li, J.; Zhang, T. *Nat. Chem.* **2011**, *3*, 634−641.

(28) McDaniel, M. P. *Adv. Catal.* **2010**, *53*, 123−606.

(29) Uzun, A.; Gates, B. C. *Angew. Chem., Int. Ed.* **2008**, *47*, 9245−9248.

(30) Lu, J.; Aydin, C.; Browning, N. D.; Gates, B. C. *J. Am. Chem. Soc.* **2011**, *133*, 16186−16195.

(31) Bayram, E.; Lu, J.; Aydin, C.; Uzun, A.; Browning, N. D.; Gates, B. C.; Finke, R. G. *ACS Catal.* **2012**, *2*, 1947−1957.

(32) (a) Watzky, M. A.; Finke, R. G. *J. Am. Chem. Soc.* **1997**, *119*, 10382−10400. and references therein; (b) Watzky, M. A.; Finke, R. G. *Chem. Mater.* **1997**, *9*, 3083−3095. (c) Aiken, J. D., III; Finke, R. G. *J. Am. Chem. Soc.* **1998**, *120*, 9545−9554 and references therein.

(33) Widegren, J. A.; Aiken, J. D., III; Özkar, S.; Finke, R. G. *Chem. Mater.* **2001**, *13*, 312−324 and references therein.

(34) Ir−C and Ir−C_{long} contributions may sometimes be counted twice when the carbon atoms are present in rings that can be tilted and

DOI: 10.1021/acscatal.5b00321
ACS Catal. 2015, 5, 3514−3527

bent on top of the Ir atoms. This complication yields higher Ir−C and/or Ir−C_{long} coordination numbers than are reflective of the structures.
(35) The time required to fully evolve to the Ir_4 clusters appears to be between 1 h and 2 days; hence, the reaction time of ∼2 days was chosen to ensure that the predominantly Ir_1/zeolite Y would evolve more fully into a higher-nuclearity, $Ir_{\geq 4}$/zeolite Y catalyst.
(36) The complete hydrogenation of 0.5 mL of cyclohexene requires ∼15 psig of H_2 under our conditions. The initial H_2 partial pressure was 40 psig, and the remaining H_2 partial pressure ∼25 psig.
(37) Argo, A. M.; Odzak, J. F.; Gates, B. C. *J. Am. Chem. Soc.* **2003**, *125*, 7107−7115.
(38) Grundwaldt, J.-D.; Kappen, P.; Basini, L.; Clausen, B. S. *Catal. Lett.* **2002**, *78*, 13−21.
(39) Li, F.; Gates, B. C. *J. Phys. Chem. B* **2003**, *107*, 11589−11596.
(40) Ortalan, V.; Uzun, A.; Gates, B. C.; Browning, N. D. *Nat. Nanotechnol.* **2010**, *5*, 506−510.
(41) Okamoto, N. L.; Reed, B. W.; Mehraeen, S.; Kulkarni, A.; Morgan, D. G.; Gates, B. C.; Browning, N. D. *J. Phys. Chem. C* **2008**, *112*, 1759−1763.
(42) Gates, B. C. *J. Mol. Catal. A: Chem.* **2000**, *163*, 55−65.
(43) The average size of the $Ir_{\sim 40}$ nanoparticles was estimated by using the equation: $n = (N_0\rho(4/3)\pi(D/2)^3)/W$,[60] where n = number of Ir atoms, $N_0 = 6.022 \times 10^{23}$ mol^{-1}, ρ = room-temperature density of iridium (22.5 g/cm^3),[43a] D = diameter of iridium nanoparticles, and W = atomic weight of iridium (192.22 g/mol). This calculation yields $Ir_{\sim 40}$ for an average diameter of ∼1.0 nm, $Ir_{\sim 70}$ for an average diameter of ∼1.3 nm, and $Ir_{\sim 50}$ and $Ir_{\sim 1600}$ for average diameters of 1.1 and 3.5 nm in the final, bimodal distribution) (a) *CRC Handbook of Chemistry and Physics*, 77th ed.; Lide, D. R., Frederikse, H. P. R., Eds.; CRC Press: Boca Raton, FL, 1996.
(44) Lu, J.; Aydin, C.; Browning, N. D.; Wang, L.; Gates, B. C. *Catal. Lett.* **2012**, *142*, 1445−1451.
(45) Such $Ir_{\sim 40}$ nanoparticles have even been observed to bounce off each other in STEM images: Aydin, C.; Lu, J.; Browning, N. D.; Gates, B. C. *Angew. Chem., Int. Ed.* **2012**, *51*, 5929−5934.
(46) Crooks, A.; Yih, K.-H.; Li, L.; Yang, J. C.; Özkar, S.; Finke, R. G. *ACS Catal.* **2015**, *5*, 3342−3353.
(47) Pawluk, T.; Hirata, Y.; Wang, L. *J. Phys. Chem. B* **2005**, *109*, 20817−20823.
(48) (a) Besson, C.; Finney, E. E.; Finke, R. G. *J. Am. Chem. Soc.* **2005**, *127*, 8179−8184. (b) Besson, C.; Finney, E. E.; Finke, R. G. *Chem. Mater.* **2005**, *17*, 4925−4938.
(49) (a) Ott, L. S.; Finke, R. G. *Chem. Mater.* **2008**, *20*, 2592−2601. (b) Shields, S.; Buhro, W. E.; Finney, E. E.; Finke, R. G. *Chem. Mater.* **2012**, *24*, 1718−1725.
(50) (a) To drive home the significance of knowing the starting point here, if it was "A", then the 2 steps and associated correct words and descriptors that should have been used to fit the data would have been bimolecular nucleation,[50b] A + A → 2B, and autocatalytic growth, A + B → 2B. Moreover, we know from experience that the associated diameter vs time equation for these two steps is very similar to eq 1 so that the fit to the observed diameter vs time data would be indistinguishable from that observed for the B + B → 2B, B + C → 1.5 C diameter equation. We have discussed previously the enormous significance to understanding chemistry and chemical mechanisms of using the proper balanced equations that not only define the rate constants, *but also define the proper words and concepts to be used* when talking about the underlying chemistry and associated mechanism.[50b,c] (b) Laxson, W. W.; Finke, R. G. *J. Am. Chem. Soc.* **2014**, *136*, 17601−17615. (c) Finney, E. E.; Finke, R. G. *Chem. Mater.* **2009**, *21*, 4692−4705.
(51) The additional approximations underlying eq 1 are (i) that the clusters are spherical so that we can relate the diameters of the clusters/nanoparticles to the number of atoms contained within them; (ii) that the rate constants k_3 and k_4 are independent of cluster/nanoparticle size (i.e., which means that the curve-fit k_3 and k_4 are average values); (iii) that the complexes/clusters at the beginning of the growth process are monodisperse, so that their concentration $[B]_0$ can be used in eq 1; because the present case started with mononuclear iridium species, this assumption is well founded; (iv) that the clusters remain monodisperse throughout the process of their formation and growth (i.e., eq 1 gives an average cluster size, but not a distribution); and (v) that the bulk metal density can be used to approximate the density of metal in the clusters/nanoparticles. One additional approximation is (vi) that an increase in the volume of the solution (resulting from the successive additions of 0.5 mL of additional cyclohexene in each cycle over and above the starting 3.0 mL of solution) is neglected. Simulations provided in the Supporting Information also show that this latter approximation does not significantly influence the fits, nor even the resultant rate constants.
(52) Breck, D. W. *Zeolite Molecular Sieves*; Wiley: New York, 1974.
(53) Tong, Y. Y.; van der Klink, J. J.; Clugnet, G.; Renouprez, A. J.; Laub, D.; Buffat, P. A. *Surf. Sci.* **1993**, *292*, 276−288.
(54) Rathousky, J.; Zukal, A.; Jaeger, N.; Schulz-Ekloff, G. *Nanostruct. Mater.* **1992**, *1*, 355−360.
(55) (a) We use the term "pseudo-elementary" as first defined by Noyes in his studies of complex, many-step oscillating reactions, that is, where one can use a reaction that is a sum of more than one elementary reaction, plus faster reactions, the sum of which is by definition a pseudo-elementary reaction that can be used in a kinetically useful way. (b) Noyes, R. M.; Field, R. J. *Acc. Chem. Res.* **1977**, *10*, 214−221. (c) Noyes, R. M.; Field, R. J. *Acc. Chem. Res.* **1977**, *10*, 273−280. (d) Field, R. J.; Noyes, R. M. *Nature* **1972**, *237*, 390−392. (e) See also our prior uses of the pseudo-elementary reaction concept in the formation and agglomeration of nanoparticles.[32,33,48,49]
(56) Wang, F.; Richards, V. N.; Shields, S. P.; Buhro, W. E. *Chem. Mater.* **2013**, *26*, 5−21.
(57) (a) Jiang, F.; Muscat, A. J. *Langmuir* **2012**, *28*, 12931−12940. (b) An, K.; Alayoglu, S.; Ewers, T.; Somorjai, G. *J. Colloid Interface Sci.* **2012**, *373*, 1−13. (c) Lilly, G. D.; Lee, J.; Sun, K.; Tang, Z.; Kim, K.-S.; Kotov, N. A. *J. Phys. Chem. C* **2008**, *112*, 370−377. (d) Qu, L.; Yu, W. W.; Peng, X. *Nano Lett.* **2004**, *4*, 465−469.
(58) Mondloch, J. E.; Finke, R. G. *J. Am. Chem. Soc.* **2011**, *133*, 7744−7756.
(59) Guo, S.; Fang, G.; Li, G.; Ma, H.; Fan, H.; Yu, L.; Ma, C.; Wu, X.; Deng, D.; Wei, M.; Tan, D.; Si, R.; Zhang, S.; Li, J.; Sun, L.; Tang, Z.; Pan, X.; Bao, X. *Science* **2014**, *344*, 616−619.
(60) Lin, Y.; Finke, R. G. *J. Am. Chem. Soc.* **1994**, *116*, 8335−8353.
(61) (a) Özkar, S.; Finke, R. G. *J. Am. Chem. Soc.* **2002**, *124*, 5796−5810. (b) Özkar, S.; Finke, R. G. *Langmuir* **2002**, *18*, 7653−7662.
(62) Wilkins, R. G. *Kinetics and Mechanism of Reactions of Transition Metal Complexes*, 2nd Ed.; VCH; Weinheim, 1991.
(63) Bhirud, V. A.; Uzun, A.; Kletnieks, P. W.; Craciun, R.; Haw, J. F.; Dixon, D. A.; Olmstead, M. M.; Gates, B. C. *J. Organomet. Chem.* **2007**, *692*, 2107−2113.
(64) Jentoft, M.; Deutsch, S. E.; Gates, B. C. *Rev. Sci. Instrum.* **1996**, *67*, 2111−2113.
(65) Newville, M.; Ravel, B.; Haskel, D.; Rehr, J. J.; Stern, E. A.; Yacoby, Y. *Phys. B* **1995**, *208/209*, 154−156.
(66) Newville, M. *J. Synchrotron Radiat.* **2001**, *8*, 96−100.
(67) Vaarkamp, M.; Linders, J. C.; Koningsberger, D. C. *Phys. B* **1995**, *209*, 159−160.
(68) Koningsberger, D. C.; Mojet, B. L.; van Dorssen, G. E.; Ramaker, D. E. *Top. Catal.* **2000**, *10*, 143−155.
(69) Zabinsky, S. E.; Rehr, J. J.; Ankudinov, A.; Albers, R. C.; Eller, M. J. *Phys. Rev. B: Condens. Matter Mater. Phys.* **1995**, *52*, 2995−3009.
(70) Pearson, W. B.; Calvert, L. D.; Villars, P. *Pearson's Handbook of Crystallographic Data for Intermetallic Phases*; American Society for Metals: Metals Park, OH, 1985.
(71) Lytle, F. W.; Sayers, D. E.; Stern, E. A. *Physica B* **1989**, *158*, 701−722.

DOI: 10.1021/acscatal.5b00321
ACS Catal. 2015, 5, 3514−3527